THE PLANT CELL

AIG2A and AIG2B limit the activation of salicylic acid-regulated defenses by tryptophan-derived secondary metabolism in Arabidopsis

Zhixue Wang [iD] ,[1] Leiyun Yang [iD] ,[1] Georg Jander [iD] ,[2] Ruchika Bhawal [iD] ,[3] Sheng Zhang [iD] ,[3] Zhenhua Liu [iD] ,[1,†] Aaron Oakley [iD] [4] and Jian Hua [iD] [1,*]

1 Plant Biology Section, School of Integrative Plant Science, Cornell University, Ithaca, New York 14853, USA
2 Boyce Thompson Institute, Ithaca, New York 14853, USA
3 Proteomics and Metabolomics Facility, Cornell University, New York 14853, USA
4 Molecular Horizons and School of Chemistry and Molecular Bioscience, University of Wollongong, New South Wales 2522, Australia

*Author for correspondence: jh299@cornell.edu
†Present address: Joint Center for Single Cell Biology; Shanghai Collaborative Innovation Center of Agri-Seeds, School of Agriculture and Biology, Shanghai Jiao Tong University, Shanghai 200240, China
These authors contributed equally (Z. W. and L. Y.)
J.H. conceived and supervised the project; J.H. and Z.W. designed the study; Z.W., L.Y., G.J., R.B., S.Z., Z.L., and A.O. conducted experiments and/or data analysis; Z.W., J.H., and G.J. wrote the manuscript with inputs from all other authors.
The author responsible for distribution of materials integral to the findings presented in this article in accordance with the policy described in the Instructions for Authors (https://academic.oup.com/plcell) is: Jian Hua (jh299@cornell.edu).

Abstract

Chemical defense systems involving tryptophan-derived secondary metabolites (TDSMs) and salicylic acid (SA) are induced by general nonself signals and pathogen signals, respectively, in *Arabidopsis thaliana*. Whether and how these chemical defense systems are connected and balanced is largely unknown. In this study, we identified the *AVRRPT2-INDUCED GENE2A* (*AIG2A*) and *AIG2B* genes as gatekeepers that prevent activation of SA defense systems by TDSMs. These genes also were identified as important contributors to natural variation in disease resistance among *A. thaliana* natural accessions. The loss of AIG2A and AIG2B function leads to upregulation of both SA and TDSM defense systems. Suppressor screens and genetic analysis revealed that a functional TDSM system is required for the upregulation of the SA pathway in the absence of AIG2A and AIG2B, but not vice versa. Furthermore, the *AIG2A* and *AIG2B* genes are co-induced with TDSM biosynthesis genes by general pathogen elicitors and nonself signals, thereby functioning as a feedback control of the TDSM defense system, as well as limiting activation of the SA defense system by TDSMs. Thus, this study uncovers an AIG2A- and AIG2B-mediated mechanism that fine-tunes and balances SA and TDSM chemical defense systems in response to nonpathogenic and pathogenic microbes.

Introduction

Plants in nature are exposed to a wide variety of pathogenic and nonpathogenic microbes. Multiple chemical defense systems are regulated in plants to maintain microbiota homeostasis and fend off pathogens ([Aerts et al., 2021](); [Paasch and](
He, 2021). A prominent chemical defense system involving tryptophan (Trp)-derived secondary metabolites (TDSMs) is broadly activated by the general recognition of both pathogenic and nonpathogenic microbes, or nonself signals ([Rajniak et al., 2015](); [Stahl et al., 2016](); [Maier et al., 2021]().

IN A NUTSHELL

Background: Plants synthesize diverse, sometimes species-specific, defensive molecules, including tryptophan-derived secondary metabolites (TDSMs) and/or salicylic acid (SA) to defend themselves. TDSMs are either toxic to invading pathogens or are able to activate downstream immune responses. They are generally produced upon recognition of nonself signals from both pathogenic and nonpathogenic microbes. By contrast, SA is induced by pathogens and activates defense responses usually at the cost of plant growth. These two chemical defense systems are thought to be largely independent. Through a genome-wide association study, we identified *AVRRPT2-INDUCED GENE2A* (*AIG2A*) and AIG2B as regulators of both TDSMs and SA chemical defense systems in *Arabidopsis thaliana*.

Questions: What is the role of AIG2A and AIG2B in regulating TDSMs and SA-mediated defense responses? Is there a connection between TDSMs and SA chemical defense systems?

Findings: In an *AIG2A* and *AIG2B* loss of function mutant (hereafter, *aig2*), the TDSMs and SA defense systems are both upregulated. Genetic removal of the TDSM biosynthesis pathway abolishes the upregulation of SA defense systems in the *aig2* mutant, but not vice versa. Thereby, AIG2A and AIG2B function as gatekeepers that prevent the activation of SA defense systems by the TDSM defense system. AIG2A and AIG2B are co-localized with TDSM biosynthetic enzymes, and their gene expression is co-induced with TDSM genes by nonself signals, suggesting a role for AIG2A and AIG2B in TDSM metabolism. In addition, putative γ-glutamyl cyclotransferase (GGCT) catalytic sites in AIG2 and AIG2 are essential for the function of these proteins in plant immunity, suggesting that the substrate (or the product) of AIG2A and AIG2B functions as an immune signaling molecule.

Next steps: We are looking for the substrate(s) of AIG2A and AIG2B through multiple approaches, including high-resolution nontargeted metabolite profiling and genetic dissections. Successful identification of these substrates will generate new insights into the interaction of the SA and the TDSM defense systems.

Nonself-induced TDSMs confer resistance to current or subsequent challenges from pathogens and maintain microbial communities associated with plants (Maier et al., 2021; Wolinska et al., 2021). In *Arabidopsis thaliana* (Arabidopsis), TDSMs are channeled through four branches of a metabolic pathway to produce camalexin, indole-3-carbonyl nitrile (ICN), indole glucosinolates (IG), and indole-3-carboxylic acid (ICA; Glawischnig, 2007; Rajniak et al., 2015). All four branches of this pathway play a critical role in defense against necrotrophic and hemibiotrophic fungal pathogens (Thomma et al., 1999; Ferrari et al., 2003; Hiruma et al., 2013; Pastorczyk and Bednarek, 2016; Müller et al., 2019; Pastorczyk et al., 2020). In addition, ICN or its derivatives are critical for defense against the hemibiotrophic bacterial pathogen *Pseudomonas syringae* (Rajniak et al., 2015), whereas IG and its derivates are involved in defense against herbivores (Agerbirk et al., 2009). Another important chemical defense system consists of salicylic acid (SA) and the mutually enhancing N-hydroxypipecolic acid (NHP; Huang et al., 2020). SA is a strong chemical defense hormone that predominantly stimulates resistance to biotrophic pathogens (Vlot et al., 2009). Pathogen-induced SA is synthesized from chorismate by ISOCHORISMATE SYNTHASE1 (ICS1), also known as SALICYLIC ACID INDUCTION DEFICIENT2 (SID2), or from phenylalanine via phenylalanine ammonia-lyases (PALs; Wildermuth et al., 2001; Huang et al., 2010; Torrens-Spence et al., 2019; Rekhter et al., 2019). NHP promotes SA biosynthesis and is synthesized from lysine by a three-step biochemical process involving AGD2-LIKE DEFENSE RESPONSE PROTEIN1 (ALD1), SAR-DEFICIENT4 (SARD4) and FLAVIN-DEPENDENT MONOOXYGENASE1 (FMO1; Ding et al., 2016; Hartmann et al., 2017; Hartmann et al., 2018; Chen et al., 2018; Liu et al., 2020). Biosynthesis of SA and NHP is induced by pathogens via the upregulation of the biosynthesis genes by two transcription factors, CALMODULIN BINDING PROTEIN 60g (CBP60g) and SARD1 (Wang et al., 2011), which are repressed by calmodulin-binding transcription factors (CAMTAs; Jing et al., 2011; Nie et al., 2012; Sun et al., 2020). It is critical for plants to ensure immune systems are activated only as needed because constitutive immune responses are costly and usually inhibit growth (Hua 2013; Wan et al., 2021). Despite the increasing efforts to elucidate the biosynthetic pathways of individual chemical defense systems, how these systems are interconnected and balanced at optimal levels is largely unknown.

More than 25 years ago, *AVRRPT2-INDUCED GENE2* (*AIG2*) was identified as a gene that is induced early after infection by *Pseudomonas syringae* pv. *tomato* (*Pst*) DC3000 carrying the *avrRpt2* avirulence gene (Reuber and Ausubel, 1996). *AIG2* has sometimes been used as a marker gene for Arabidopsis responses to *Pst* DC3000, but its function has been enigmatic. The encoded protein is in a plant-specific γ-glutamyl cyclotransferase (psGGCT) subfamily of the GGCT-like superfamily (GGCT-like; Kumar et al., 2015). GGCT-like proteins catalyze the production of 5-oxo-proline from γ-glutamyl-containing small molecules (Oakley et al., 2008, 2010). In addition to the psGGCT subfamily, Arabidopsis has two other GGCT-like subfamilies: ChaC and

GGACT (Kumar et al., 2015). The well-characterized ChaC proteins preferentially catalyze the breakdown of glutathione (GSH). They function in sulfur starvation responses (Joshi et al., 2019) and in detoxification of heavy metals and metalloids in Arabidopsis (Paulose et al., 2013). However, the function of AIG2 or psGGCT subfamily proteins remains unclear.

In this study, we identified AIG2 as an immunity regulator in Arabidopsis through a genome-wide association study (GWAS). The loss-of-function mutant of AIG2 (hereafter AIG2A) and its close homologs, AIG2B and AIG2C, has enhanced resistance to Pst DC3000 but reduced resistance to Penicillium. Biosynthesis of SA and NHP, as well as camalexin and other TDSMs, is upregulated in the aig2a aig2b aig2c (referred to as aig2abc) triple mutant. Interestingly, a functional TDSM system is required for the upregulation of SA-NHP in the aig2abc mutant, indicating an activation of SA-NHP by TDSMs in the absence of AIG2A and AIG2B. Furthermore, AIG2A and AIG2B proteins are co-localized with TDSM biosynthetic enzymes, and the corresponding gene expression is co-induced by general pathogen elicitors. Therefore, our study uncovers a critical role for AIG2A and AIG2B in preventing the activation of SA-NHP by TDSMs. This could be a critical regulatory mechanism that modulates SA-NHP immune response activation by nonself recognition and signaling.

Results

Loss of AIG2A and AIG2B function leads to enhanced resistance to Pst DC3000

To identify genes responsible for natural variation in resistance to Pst DC3000, we performed a GWAS of Pst DC3000 growth in 100 Arabidopsis natural accessions (Supplemental Data Set S1; Wang et al., 2019). One significant peak of associated SNPs was found at 1,096 kbp on chromosome 3 (Supplemental Figure S1) in a gene cluster containing AIG2A (AT3G28930), AIG2B (AT3G28940), and AIG2C (AT3G28950;

Supplemental Figure S1). Sequence searches with AIG2A, AIG2B, and AIG2C revealed four other close homologs in Arabidopsis (Figure 1A). Based on their protein sequences, these genes can be divided into three groups, namely AIG2-I (AIG2A, AIG2B, and AIG2C), AIG2-II (AIG2LA and AIG2LB), and AIG2-III (AIG2LC and AIG2LD; Figure 1A).

To establish the function of the AIG2-I gene family, we generated single and higher order mutants of these three genes using CRISPR/Cas9 (Wang et al., 2015). These included single-mutant alleles of AIG2A, AIG2B, and AIG2C; double mutant combinations for AIG2A and AIG2B; and triple mutants of all three genes (Supplemental Figure S2, A and B). All of these mutations are likely knockouts, as indicated by the predicted truncation of the proteins or the absence of mRNA transcripts (Supplemental Figure S2, B and C). None of the single mutants exhibited obvious defects in rosette leaf growth compared to the wild-type Col-0 (hereafter WT; Figure 1B). However, the aig2a aig2b (referred to as aig2ab) double mutants and the aig2abc triple mutants were smaller in rosette size than the WT and were similar to one another (Figure 1B). When infected with Pst DC3000, the aig2ab and aig2abc mutants had lower pathogen growth compared to the WT, whereas the single mutants aig2a, aig2b, and aig2c had comparable pathogen growth to the WT (Figure 1C; Supplemental Figure S3A). In addition, cloned AIG2A (pAIG2A:AIG2A) and AIG2B (pAIG2B:AIG2B), but not AIG2C (pAIG2C:AIG2C), complemented the growth and immunity phenotypes of the aig2abc-1 (hereafter aig2abc) mutant (Supplemental Figure S3, B and C). Together, these results demonstrate that AIG2A and AIG2B, but not AIG2C, regulate plant growth and immunity.

The SNPs associated with Pst DC3000 resistance in the GWAS resided in the promoter region of AIG2A, as well as the promoter, 3′UTR, and coding regions of AIG2B (Supplemental Figure S1), suggesting that natural variation regulates the expression of these genes. Indeed, expression variation in AIG2A and AIG2B was also observed in 665 natural accessions of Arabidopsis (Kawakatsu et al., 2016).
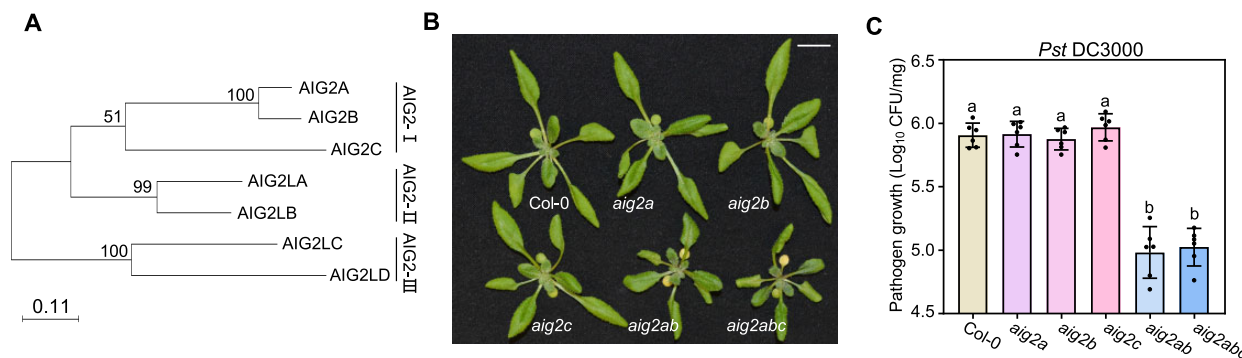
Figure 1 Loss of AIG2A and AIG2B function confers enhanced resistance to Pst DC3000. A, Phylogenetic tree of the Arabidopsis AIG2 family proteins. The maximum likelihood tree generated from multiple sequence alignment of the amino acid sequences in seven Arabidopsis AIG2 family proteins using Mega-X is shown. Tree branch lengths indicate the number of substitutions per site. Bootstrap supporting values (>50, 1,000 bootstraps) are shown next to the branches. B, Morphology of Col-0, aig2a-1 (aig2a), aig2b-1 (aig2b), aig2c-1 (aig2c), aig2ab-2 (aig2ab), and aig2abc-1 (aig2abc) plants grown under constant light for 3 weeks. Scale bar, 1 cm. C, Growth of the bacterial pathogen Pst DC3000 in plants shown in (B) at 3 d post-infection. Error bars represent the SD of six biological replicates. Different letters indicate significant differences (P < 0.05) tested by one-way ANOVA with Duncan's post hoc test.

Expression GWAS (eGWAS) revealed that *AIG2A* expression variation in natural Arabidopsis accessions was strongly associated with the *AIG2A* locus itself, especially the promoter region (Supplemental Figure S4A). Similarly, *AIG2B* expression was significantly associated with the *AIG2B* gene itself (Supplemental Figure S4B). These data suggest that natural polymorphisms in the AIG2 cluster contribute to expression variation in the *AIG2A* and *AIG2B* genes and consequently affect the disease resistance of Arabidopsis accessions.

It is also possible that structural variations that cannot be detected by resequencing of natural accessions exist in the *AIG2* region, especially due to the presence of a retrotransposon element. Some of these structural variations may generate natural loss of one or more *AIG2* genes in this region. Examination of these three genes in the eight Arabidopsis accessions that have *de novo* sequenced genomes did not identify any obvious loss of these genes. Comprehensive resequencing of this region in additional accessions will be needed to investigate this possibility.

AIG2A and AIG2B are induced by nonself signals and are co-expressed with TDSM genes

To better understand the function of *AIG2A* and *AIG2B*, we analyzed the expression regulation of *AIG2*-I genes in detail.

Genes co-expressed with *AIG2*-I genes under diverse growth and environmental conditions were identified with an average logit score $\geqslant 3$ using a web-based tool ATTED-II (https://atted.jp/coexsearch/). The top 100 positively co-expressed genes with *AIG2A* were enriched in GO terms related to Trp and TDSM biosynthetic pathways (Figure 2A; Supplemental Data Set S2). *AIG2B*, but not *AIG2C*, was co-expressed with genes enriched in the same GO terms as *AIG2A* (Figure 2B). Closer examination of the transcriptome database (Zhang et al., 2020) revealed that biotic stresses were the most prominent factors that induced the expression of *AIG2A* and *AIG2B*. The transcripts of both *AIG2A* and *AIG2B* were induced by the virulent strain *Pst* DC3000, as well as the avirulent strains *Pst* DC3000 (avrRpm1) and *Pst* DC3000 (avrRpt2; Figure 2C; Mine et al., 2018). A panel of seven immune-triggering molecular patterns, including flg22 (22-aa peptide derived from flagellin), elf18 (18-aa peptide from EF-Tu), Pep1, nlp20, oligogalacturonides, chitooligosaccharide 8 and 3-hydroxy fatty acids, also induced the transcripts of these two genes, with *AIG2A* generally having a greater induction (Figure 2C; Bjornson et al., 2021). In addition, SA induced the transcription of *AIG2A*, but not *AIG2B*, at 1 h after treatment (Supplemental Figure S5A; Ding et al., 2018). A similar expression induction pattern
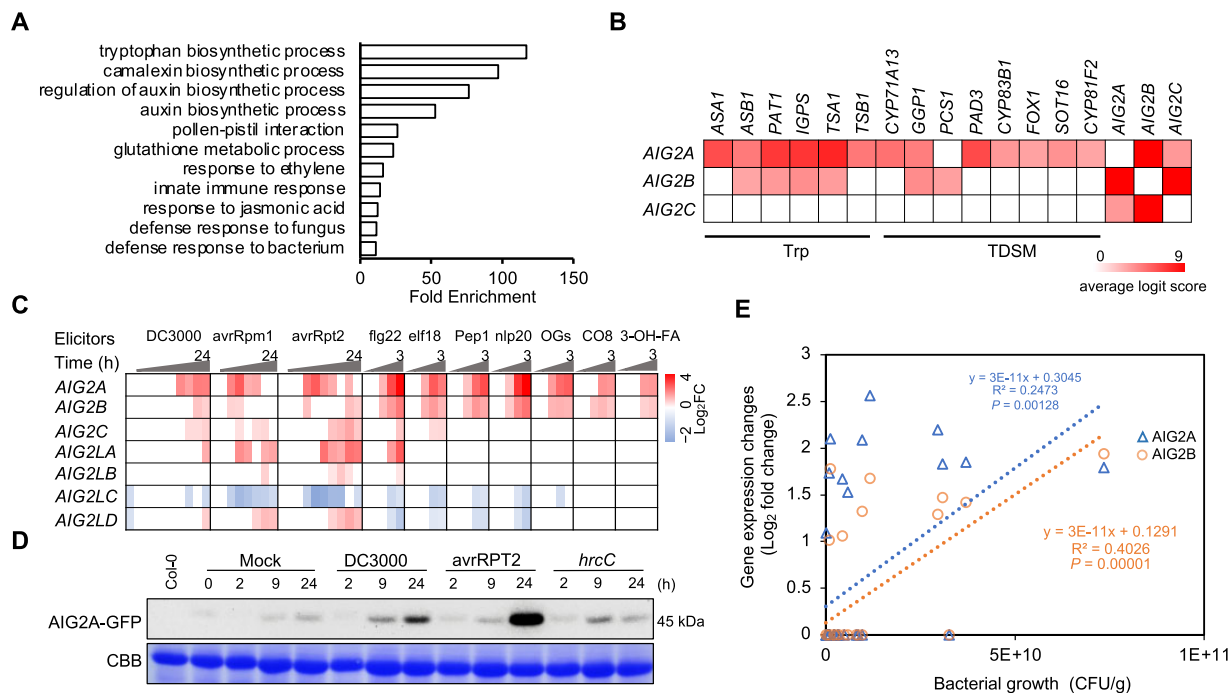
Figure 2 AIG2-I genes are induced by biotic stresses and co-expressed with biosynthesis genes of Trp and TDSMs. A, GO analysis of the top 100 co-expressed genes of *AIG2A* extracted from ATTED-II version 11. B, Co-expressed genes of *AIG2A*, *AIG2B*, and *AIG2C* involved in biosynthetic pathways of Trp and TDSMs. Shown are the average logit scores from ATTED-II version 11. C, RNA expression of AIG2 family genes in response to elicitors in a time-course analysis extracted from two publicly available RNA-seq datasets. Shown are the log₂ transformed fold changes at the indicated time points. D, Immunoblot detecting an AIG2A-GFP fusion protein using anti-GFP antibodies in a *pAIG2A:AIG2A-GFP* transgenic line in the *aig2abc-1* mutant background after inoculation with a virulent strain (DC3000), an avirulent strain (avrRpt2), and a nonvirulent strain (*hrcC*) of *Pst* DC3000 at 2 h, 9 h, and 24 h post-inoculation. CBB, Coomassie brilliant blue. E, Correlation of phyllosphere colonization of nonpathogenic bacteria with RNA expression changes in *AIG2A* and *AIG2B* genes in response to these bacteria. Linear regressions of the bacterial growth against expression changes in *AIG2A* and *AIG2B* genes are shown. Coefficients of variation from the linear regression value (R^2) are provided. RNA-seq data were retrieved from Maier et al. (2021).

was also observed for the *AIG2A*. An AIG2A-GFP fusion protein, encoded by a transgene expressed under the native *AIG2A* promoter, was induced by *Pst* DC3000 strains and flg22 (Figure 2D; Supplemental Figure S5B). Among all *AIG2*-like genes, strong induction by pathogens and molecular patterns appeared to be specific for *AIG2A* and *AIG2B* (Figure 2C).

RNA-seq experiments showed that TDSM biosynthesis genes are enriched among genes induced by nonpathogenic leaf colonizing bacteria (Maier et al., 2021). We, therefore, used this dataset to analyze the expression of *AIG2A* and *AIG2B* in response to infection by nonpathogenic bacteria (Maier et al., 2021). *AIG2A* and *AIG2B*, respectively, were induced by 11 and 9 out of 39 tested bacterial strains (Figure 2E), which placed them among the top 300 and top 500 most frequently induced genes in these experiments (Maier et al., 2021). Interestingly, the colonization ability of the bacterial strains in the phyllosphere was positively correlated with the expression induction of *AIG2A* (R^2 = 0.25, P = 0.00128) and *AIG2B* (R^2 = 0.40, P = 0.00001; Figure 2E), as well as the number of induced TDSM biosynthesis genes (R^2 = 0.2053, P = 0.00378). This suggests that bacteria with higher colonization ability tend to induce expression of *AIG2A* and *AIG2B*, as well as a greater number of TDSM biosynthesis genes.

Taken together, these results indicate that *AIG2A* and *AIG2B* are induced by nonself signals associated with both nonpathogenic and pathogenic microbes, and that the extent of *AIG2A* and *AIG2B* induction is likely proportional to the level of nonself signals detected by the plant.

### *AIG2-I* genes repress SA- and NHP-mediated defense responses

To understand how *AIG2*-I genes regulate plant immunity, we performed suppressor screens on the *aig2abc* mutant to identify important genes mediating the defense responses. Causal mutations for five suppressors were identified using a mapping-by-sequencing method (Hua et al., 2017). Two suppressors harbored mutations in genes (*CAMTA3* and *SID2*) that are involved in SA and NHP biosynthesis

(Supplemental Figure S6, A–C). These two mutants, *camta3*[D] and *sid2-6*, rescued the growth and immunity phenotypes of the *aig2abc* mutant (Figure 3, A and B). A commonly used knockout allele *sid2-1* (hereafter *sid2*; Nawrath and Métraux, 1999) also led to a WT-like growth and resistance phenotype when introduced into the *aig2abc* mutant (Figure 3, C and D). In addition, a mutation in *FMO1*, which blocks NHP biosynthesis, was able to revert the growth and immunity phenotypes of the *aig2abc* mutant (Figure 3, C and D). These results indicate that activation of SA-NHP biosynthesis is likely the cause of the pathogen resistance and growth phenotypes of the *aig2abc* mutant.
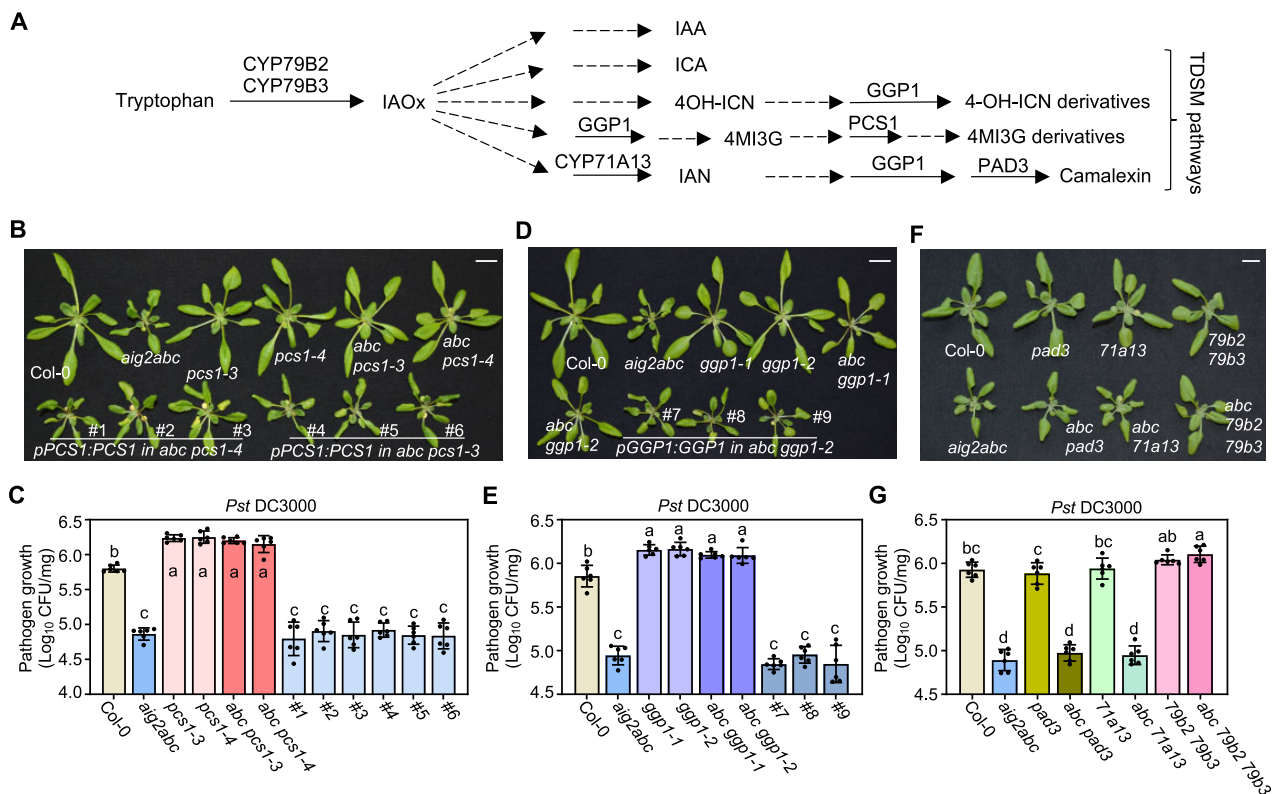
TDSM biosynthesis genes are required for enhanced resistance to *Pst* DC3000 in the *aig2abc* mutant

The suppressor screen also revealed that a functional TDSM system is essential for the enhanced resistance in the *aig2abc* mutant. Mutations of two TDSM genes, *PHYTOCHELATIN SYNTHASE 1* (*PCS1*) and *γ-GLUTAMYL PEPTIDASE 1* (*GGP1*), reverted the enhanced disease resistance phenotype of *aig2abc* (Figure 4, A–C). *PCS1* encodes a bifunctional enzyme with GSH γ-glutamyl-cysteinyl-transferase activity and glycine-cleaving peptidase activity on GSH conjugates (Figure 4A; Hématy et al., 2020). The two independent mutations (*pcs1-3* and *pcs1-4*) resulted in premature stop codons at amino acids 80 and 399, respectively (Supplemental Figure S6D). The identification of *PCS1* as the casual gene of the suppressors was further verified by a complementation test where the wild-type genomic fragment of *PCS1* (*pPCS1:PCS1*) was able to revert the growth and immunity phenotypes of both *aig2abc pcs1-3* and *aig2abc pcs1-4* mutants to that of *aig2abc* (Figure 4, B and C).

The second gene encodes a γ-glutamyl peptidase (GGP1) that hydrolyzes the γ-glutamyl bond of GSH conjugates (Figure 4A; Geu-Flores et al., 2009). The suppressor mutation, named *ggp1-2*, caused a premature stop codon at amino acid 41 of GGP1 (Supplemental Figure S6D). The identification of *GGP1* as the suppressor gene was verified by both a complementation test and second allele analysis
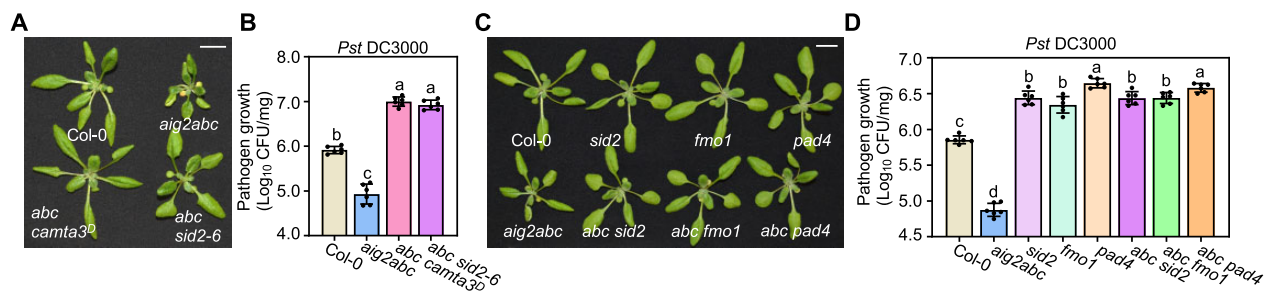
Figure 3 SA and NHP biosynthesis is critical for enhanced resistance to *Pst* DC3000 in the *aig2abc* mutant. A, Morphology of Col-0, *aig2abc-1* (*aig2abc*), *aig2abc camta3*[D] (*abc camta3*[D]), and *aig2abc sid2-6* (*abc sid2-6*) plants grown under constant light for 3 weeks. B, Growth of the bacterial pathogen *Pst* DC3000 in plants shown in (A) at 3 d post-infection. C, Morphology of Col-0, *aig2abc*, *sid2-1* (*sid2*), *fmo1-1* (*fmo1*), *pad4-1* (*pad4*), *aig2abc sid2* (*abc sid2*), *aig2abc fmo1* (*abc fmo1*), and *aig2abc pad4* (*abc pad4*) plants grown under constant light for 3 weeks. D, Growth of the bacterial pathogen *Pst* DC3000 in plants shown in (C) at 3 d post-infection. Scale bars, 1 cm. Error bars represent the SD of six biological replicates. Different letters indicate significant differences (P < 0.05) tested by one-way ANOVA with Duncan's post hoc test.

Figure 4 Biosynthetic enzymes for TDSMs are required for enhanced resistance to *Pst* DC3000 in the *aig2abc* mutant. A, Simplified scheme of biosynthetic pathways of TDSMs and the reported functions of CYP79B2, CYP79B3, CYP71A13, PCS1, GGP1, and PAD3 in these pathways. Dashed arrows indicate multiple biochemical reaction steps and solid arrows indicate a single biochemical reaction step. IAA: indole-3-acetate; ICA: indole-3-carboxylic acid; 4OH-ICN: 4-hydroxy-indole-3-carbonyl nitrile; 4MI3G: 4-methoxy-3-indolylmethyl-IG; IAN: indole-3-acetonitrile. B, Morphology of Col-0, *aig2abc-1* (*aig2abc*), *pcs1-3*, *pcs1-4*, *aig2abc pcs1-3* (*abc pcs1-3*), and *aig2abc pcs1-4* (*abc pcs1-4*) plants as well as plants from three independent representative lines of *pPCS1:PCS1* in *abc pcs1-4* (#1, #2 and #3) and *pPCS1:PCS1* in *abc pcs1-3* (#4, #5, and #6) at 3 weeks old grown under constant light. C, Growth of the bacterial pathogen *Pst* DC3000 in plants shown in (B) at 3 d post-infection. D, Morphology of Col-0, *aig2abc*, *ggp1-1*, *ggp1-2*, *aig2abc ggp1-1* (*abc ggp1-1*), and *aig2abc ggp1-2* (*abc ggp1-2*) plants as well as plants from three independent representative lines of *pGGP1:GGP1* in *abc ggp1-2* (#7, #8, and #9) at 3 weeks old grown under constant light. E, Growth of the bacterial pathogen *Pst* DC3000 in plants shown in (D) at 3 d post-infection. F, Morphology of Col-0, *aig2abc*, *pad3*, *cyp71a13* (*71a13*), *cyp79b2 cyp79b3* (*79b2 79b3*), *aig2abc pad3* (*abc pad3*), *aig2abc 71a13* (*abc 71a13*), and *aig2abc 79b2 79b3* (*abc 79b2 79b3*) plants at 3 weeks old grown under constant light. G, Growth of the bacterial pathogen *Pst* DC3000 in plants shown in (F) at 3 d post-infection. Scale bars, 1 cm. Error bars represent the SD of six biological replicates. Different letters indicate significant differences ($P < 0.05$) tested by one-way ANOVA with Duncan's post hoc test.

(Figure 4, D and E). The wild-type fragment of *GGP1* (pGGP1:GGP1) fully reverted the growth and immunity phenotypes of the *aig2abc ggp1-2* mutant to that of *aig2abc* (Figure 4, D and E), and a T-DNA insertion loss-of-function mutant allele *ggp1-1* suppressed the growth defects and disease resistance phenotype of the *aig2abc* mutant (Figure 4, D and E). These results demonstrate that *PCS1* and *GGP1* are both required for the enhanced defense response of the *aig2abc* mutant against *Pst* DC3000.

Blocking the entry reaction of TDSM biosynthesis compromises the enhanced resistance to *Pst* DC3000 in the *aig2abc* mutant

GGP1 and *PCS1* have been implicated in catabolism of GSH conjugates in multiple TDSM biosynthetic pathways, including camalexin, ICN, and IG (Figure 4A; Clay et al., 2009; Geu-Flores et al., 2011; Møldrup et al., 2013; Hématy et al., 2020). This suggests that one or multiple TDSMs might be involved

in the activation of SA-NHP defenses in the *aig2abc* mutant. We tested whether blocking the entry reaction of the TDSM biosynthetic pathways could inhibit the defense activation in the *aig2abc* mutant. Mutations of *CYP79B2* and *CYP79B3*, which encode enzymes converting Trp to indole-3-acetaldoxime (IAOx), the precursor for all TDSMs (Figure 4A; Mikkelsen et al., 2000; Zhao et al., 2002), were simultaneously introduced into the *aig2abc* mutant. The *aig2abc cyp79b2 cyp79b3* quintuple mutant had a larger rosette and was more susceptible to *Pst* DC3000 infection than the *aig2abc* triple mutant (Figure 4, F and G), indicating that biosynthesis of IAOx is required for *aig2abc*-induced immunity.

We further tested whether camalexin, a TDSM, is required for *aig2abc*-induced immunity. Camalexin is essential for defense against necrotrophic and hemibiotrophic fungi (Thomma et al., 1999; Ferrari et al., 2003; Hiruma et al., 2013; Pastorczyk et al., 2020), but has a minimal direct role

in defense against the bacterial pathogen *Pseudomonas syringae* (Glazebrook et al., 1997; Zhou et al., 1999). *CYP71A13* and *PAD3* mutations were introduced into the *aig2abc* mutant to specifically block camalexin biosynthesis (Figure 4A; Zhou et al., 1999; Nafisi et al., 2007). Neither mutation altered the growth or immunity phenotypes of the *aig2abc* mutant (Figure 4, F and G), indicating that camalexin biosynthesis by itself is not required for the enhanced *Pst* DC3000 resistance in the *aig2abc* mutant.

Biosynthesis of Trp and TDSMs as well as SA and NHP is increased in the *aig2abc* mutant

To further elucidate how *AIG2*-I genes regulate plant immunity, we performed RNA-sequencing (RNA-seq) analyses to

reveal transcriptome changes in the *aig2abc* triple mutant. A total of 2,043 and 3,352 differentially expressed genes (DEGs) were upregulated (up-DEGs) and downregulated (down-DEGs), respectively, in the *aig2abc* mutant compared to in the WT (Supplemental Data Set S3). Gene ontology (GO) analysis revealed that up-DEGs were enriched in GO terms related to metabolic processes and defense-related processes and down-DEGs were enriched in GO terms related to photosynthesis (Supplemental Figure S7, A and B).

One of the top enriched GO terms for up-DEGs was "indole-containing compound biosynthetic process" which is associated with TDSM biosynthesis (Supplemental Figure S7). We analyzed the expression of all genes known to function in the TDSM biosynthetic pathways (Figure 5A;
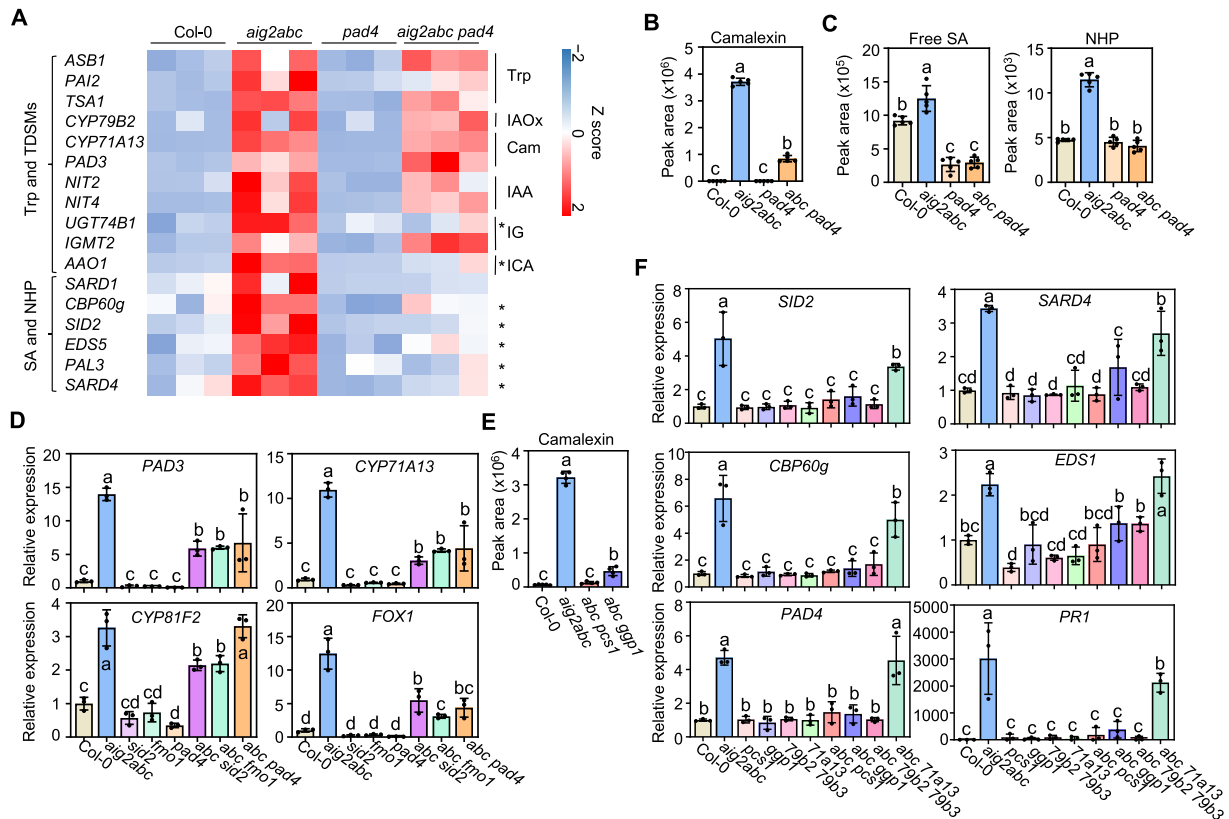
Figure 5 A functional TDSM system is required for SA-NHP biosynthesis but not vice versa in the *aig2abc* mutant. A, Expression levels of DEGs in biosynthetic pathways of Trp, IAOx, camalexin (Cam), ICA and IAA, biosynthetic or catabolic pathways of indole IG, and biosynthesis of SA and NHP in the *aig2abc-1* (*aig2abc*) mutant and the *aig2abc pad4* mutant. Expression levels were extracted from RNA-seq data, and genes with a normalized read count > 10 are shown. Colors represent Z-score normalized values. Each square indicates one biological replicate and values from three biological replicates are shown. "*" indicates a significant difference in expression levels between *aig2abc pad4* and *aig2abc* tested by Student's t test (P < 0.05). B and C, Relative content of camalexin (B), free SA and NHP (C) in whole seedlings of Col-0, *aig2abc*, *pad4*, and *aig2abc pad4* (*abc pad4*) at 3 weeks old when grown under constant light. Shown are the peak areas captured by HPLC-MS. D, Expression of *PAD3*, *CYP71A13*, *CYP81F2*, and *FOX1* genes in wild-type Col-0, *aig2abc*, *sid2*, *fmo1*, *pad4*, *abc sid2*, *abc fmo1*, and *abc pad4* plants at 4 weeks old when grown under 12-h light/12-h dark conditions. Shown are relative expression levels analyzed by RT-qPCR using *ACTIN2* as a reference gene; expression was normalized to that in wild-type Col-0. E, Relative content of camalexin in whole seedlings of Col-0, *aig2abc*, *aig2ab1 pcs1-4* (*abc pcs1*), and *aig2abc ggp1-2* (*abc ggp1*) at 3 weeks old when grown under constant light. Shown are the peak areas captured by HPLC-MS. F, Expression of *SID2*, *SARD4*, *CBP60g*, *EDS1*, *PAD4*, and *PR1* genes in Col-0, *aig2abc*, *pcs1*, *ggp1*, *79b2 79b3*, *71a13*, *abc pcs1*, *abc ggp1*, *abc 79b2 79b3*, and *abc 71a13* plants at 4 weeks old when grown under 12-h light/12-h dark conditions. Shown are relative expression levels analyzed by RT-qPCR using *ACTIN2* as a reference gene; expression was normalized to that in wild-type Col-0. Error bars represent the SD of five biological replicates for (B and C), four biological replicates for (E), and three biological replicates for (D and F). Different letters indicate significant differences (P < 0.05) tested by one-way ANOVA with Duncan's post hoc test.

Supplemental Figures S8 and S9) and found each of the four pathways had genes upregulated in the *aig2abc* mutant, including two out of six for camalexin, five out of twelve for IG, one out of three for ICN, and one out of two for ICA (Supplemental Figure S8A). Consistently, camalexin accumulated to a high level in the *aig2abc* mutant compared to in the WT (Figure 5B). Up-DEGs were also enriched in the GO terms "toxin catabolic process" and "glutathione metabolic process." Closer examination of DEGs under these terms revealed that they included multiple genes that encode GSH S-transferases (Wagner et al., 2002), which are required for biosynthesis of GSH conjugates in multiple TDSM biosynthetic pathways (Supplemental Figure S8B). These data suggest that loss of AIG2-I function upregulates the expression of genes involved in TDSM biosynthetic pathways. In addition, 5 of the 13 genes in the Trp biosynthetic pathway, one of the two homologous genes in IAOx biosynthesis, and two out of the five genes in the IAOx-derived IAA biosynthetic pathway were also upregulated in the *aig2abc* mutant (Supplemental Figure S8A). These results indicate that the loss of *AIG2*-I function also increases expression of biosynthesis genes for Trp and IAOx, which are precursors of TDSMs.

Up-DEGs in the *aig2abc* mutant were also enriched in multiple defense-related GO terms (Supplemental Figure S7A). Because SA and NHP biosynthesis was required for the enhanced resistance to *Pst* DC3000 in the *aig2abc* mutant (Figure 3), we examined the expression of SA and NHP biosynthesis genes and their regulators in the *aig2abc* mutant in detail. Transcription factors that regulate SA-NHP biosynthesis (*CBP60g* and *SARD1*), SA biosynthesis genes (*SID2* and *PAL3*), and an NHP biosynthesis gene (*SARD4*) were all upregulated in the *aig2abc* mutant (Figure 5A; Supplemental Figure S8A). Consistent with these gene expression changes, free SA and NHP have higher accumulation in the *aig2abc* mutant than in the WT (Figure 5C). Taken together, these data indicate that the loss of AIG2-I function triggers biosynthesis of SA and NHP, thereby activating SA-NHP-mediated defenses.

Activation of TDSM biosynthesis in the *aig2abc* mutant is largely independent of SA-NHP

As both the TDSM and SA-NHP chemical systems were upregulated in the *aig2abc* mutant (Figure 5, A–C), we next tested whether TDSM activation requires SA-NHP. We used *sid2* and *fmo1* to block the biosynthesis of SA and NHP, respectively, and compared expression of TDSM biosynthesis genes in the *aig2abc sid2* and *aig2abc fmo1* mutants with that in the *aig2abc* mutant. Camalexin biosynthesis genes *PAD3* and *CYP71A13*, IG biosynthesis gene *CYP81F2*, and ICN biosynthesis gene *FOX1* all had increased expression in the *aig2abc* mutant compared to in the WT. Their expression in the *aig2abc sid2* and *aig2abc fmo1* mutants was reduced compared to that in the *aig2abc* mutant but was much higher than that in the WT (Figure 5D). This indicates that the SA-NHP system is not required for the upregulation

of TDSM biosynthesis genes in the *aig2abc* mutant, although it enhances their expression.

We further used the *pad4* mutation to block the SA-NHP defense system, as *PAD4* is required for SA-NHP biosynthesis and signaling (Zhou et al., 1998; Jirage et al., 1999; Bauer et al., 2021). The *pad4* mutation resulted in a stronger suppression of the defects in the *aig2abc* mutant than the *sid2* or *fmo1* mutations, fully alleviating the growth defects and reverting the elevated *Pst* DC3000 resistance of the *aig2abc* mutant (Figure 3, C and D). The high accumulation of both free SA and NHP in the *aig2abc* mutant was also abolished by the *pad4* mutation (Figure 5C). RNA-seq analysis was carried out on the *aig2abc pad4* mutant to reveal transcriptome changes in the *aig2abc* mutant in the absence of SA-NHP defense activation. As expected, the *pad4* mutation greatly reduced the expression of SA and NHP biosynthesis genes (*SID2*, *PAL3*, and *SARD4*), as well as biosynthesis-regulating genes (*CBP60g* and *SARD1*), in the *aig2abc* mutant (Figure 5A). We, therefore, tested whether the TDSM biosynthetic pathways were activated in the *aig2abc pad4* mutant, in which the SA-NHP pathway is blocked. Up-DEGs of *aig2abc pad4* compared to *pad4* were enriched in GO terms including "camalexin biosynthetic process," "indole glucosinolate metabolic process," and "Trp biosynthetic process" (Supplemental Figure S10; Supplemental Data Set S4), indicating that TDSM pathways were activated even with the removal of SA-NHP activation. Consistent with the gene expression pattern, camalexin accumulated to a higher level in the *aig2abc pad4* mutant compared to in the WT but to a lesser extent than that in the *aig2abc* mutant (Figure 5B).

Taken together, these results indicate that upregulation of TDSM biosynthetic pathways is not dependent on *PAD4*-mediated SA and NHP activation, and that the upregulation of Trp and TDSM biosynthesis in the *aig2abc* mutant is largely independent of SA-NHP biosynthesis and signaling.

Blocking TDSM biosynthetic pathways inhibits the activation of SA biosynthesis in the *aig2abc* mutant

Genetic data indicate that the upregulation of the SA-NHP pathway in the *aig2abc* mutant is dependent on the TDSM biosynthetic pathways. We further examined gene expression to gain a better understanding of which TDSMs might be responsible for the upregulation of the SA-NHP pathway. Four mutations in the TDSM pathways were used to block the biosynthesis of all or specific pathways. They include the *cyp79b2* and *cyp79b3* mutations (*cyp79b2 79b3*) to block the IAOx biosynthesis in the entry reaction of TDSM biosynthetic pathways, the *pcs1-4* (hereafter *pcs1*) and *ggp1-2* (hereafter *ggp1*) mutations to block the breakdown reactions of GSH conjugates in multiple TDSM biosynthetic pathways, and the *cyp71a13* mutation to block the initial steps of camalexin biosynthesis. Camalexin accumulation was largely reduced in the *aig2abc pcs1* and *aig2abc ggp1* quadruple mutant compared to in the *aig2abc* triple mutant, and the *aig2abc pcs1* mutant had a comparable

camalexin level to the WT (Figure 5E). Biosynthesis genes of SA and NHP, as well as their regulators and reporters, including *SID2*, *SARD4*, *CBP60g*, *PAD4*, *EDS1*, and *PR1*, all had increased expression in the *aig2abc* mutant compared to in the WT. Furthermore, the expression of all of these genes was decreased in the *aig2abc cyp79b2 cyp79b3*, *aig2abc pcs1*, and *aig2abc ggp1* mutants compared to in the *aig2abc* mutant to levels comparable to the WT expression levels (Figure 5F). In contrast to mutations of *cyp79b2 cyp79b3*, *pcs1*, and *ggp1*, mutation of *cyp71a13*, which affects camalexin specifically, did not alter expression of *PAD4* or *EDS1* in the *aig2abc* mutant, and it reduced expression of *SID2*, *SARD4*, *CBP60g*, and *PR1* in the *aig2abc* mutant but not to the WT level (Figure 5F). These data indicate that activation of multiple TDSM biosynthetic pathways, including camalexin, is required for the upregulation of SA-NHP biosynthesis in the *aig2abc* mutant (Figure 6A).
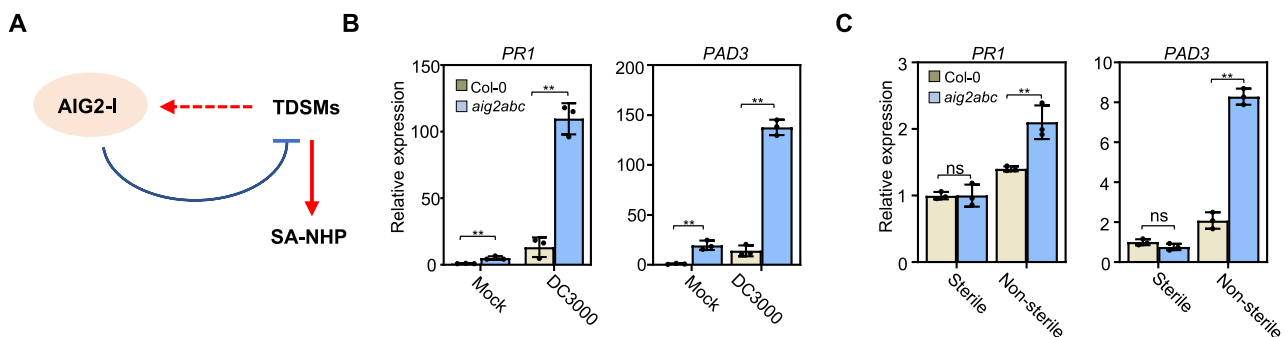
AIG2A and AIG2B repress TDSM and SA pathways in the presence of pathogens and nonpathogenic microbes

Because *AIG2*-I genes are induced by both pathogenic and nonpathogenic organisms, we investigated whether they function in the presence of microbes but not under aseptic conditions. Up to now, all experiments were done in lab conditions where plants were not grown aseptically and would have harbored nonpathogenic organisms. Under this nonpathogen infection condition, *AIG2A* and *AIG2B* repress biosynthesis of TDSM and SA-NHP, as shown by the autoimmune phenotype in the *aig2abc* mutant (Figure 5). We examined whether they influence the SA-NHP signaling and TDSM biosynthetic pathways during pathogen infection. Both pathways were upregulated in response to *Pst* DC3000, as indicated by the increased expression of *PR1* and *PAD3* at 24 h after infection (Figure 6B). The *aig2abc* mutant had higher expression of *PR1* and *PAD3* than the WT prior to infection and continued to have a higher expression after pathogen infection (Figure 6B). This suggests that *AIG2*-I

genes also repressed SA-NHP signaling and TDSM biosynthetic pathways during pathogen infection. We further asked whether *AIG2*-I genes influence SA-NHP and TDSM systems under sterile conditions, where they do not have high expression levels (Maier et al., 2021). When grown on sterile solid medium, the WT had very low *PR1* and *PAD3* expression levels and the *aig2abc* mutant had comparable expression of these two genes (Figure 6C). This suggests that *AIG2*-I genes have a significant function in repressing defense systems under nonsterile conditions, where they can be induced by both pathogens and nonpathogens, together with TDSM genes.

AIG2-I genes promote plant resistance to *Penicillium* sp. by repressing the SA-NHP pathway

Because *AIG2*-I genes are upregulated by pathogens and block activation of the SA-NHP pathway, we asked whether they might promote resistance to pathogens with a chemical defense requirement that is different from the bacterial pathogen *Pst* DC3000. The *aig2abc* mutant did not exhibit a significantly different resistance level to *Botrytis cinerea* or *Alternaria brassicicola* compared to the WT (Supplemental Figure S11), but it exhibited strong necrotic lesions in response to a natural infection that did not occur in the WT (Figure 7, A and B). The causative pathogens were identified as two species in the *Penicillium* genus. The resistance of the *aig2abc* mutant against these two fungi species was verified by drop inoculation and quantification of lesion size 7 d after inoculation. The *aig2abc* mutant had larger lesion sizes and was more susceptible to these two *Penicillium* species than the WT (Figure 7, A–C). RT-qPCR analysis revealed that *AIG2A* but not *AIG2B* was induced at 1-d post-inoculation (dpi) with *Penicillium* sp. pv. *At1* (abbreviated as *PeAt1*; Figure 7D). Interestingly, *PAD3* expression was induced 1.7-fold by *PeAt1*, whereas *PR1* expression did not change (Figure 7D), suggesting that the SA-NHP signaling pathway is repressed in the WT after infection.

Figure 6 AIG2A and AIG2B repress TDSM and SA pathways in the presence of pathogens and nonpathogenic microbes. A, Working model for the role of AIG2-I genes in regulating TDSM and SA-NHP defense systems. AIG2-I genes inhibit TDSM biosynthesis and the consequent SA-NHP biosynthesis activated by TDSMs. B, Expression of *PR1* and *PAD3* genes in Col-0 and *aig2abc* plants at 24 h post-inoculation with *Pst* DC3000. Shown are relative expression levels analyzed by RT-qPCR using *ACTIN2* as a reference gene; expression was normalized to that in the wild-type Col-0 with Mock treatment. C, Expression of *PR1* and *PAD3* genes in Col-0 and *aig2abc* plants under sterile conditions. Shown are relative expression levels analyzed by RT-qPCR using *ACTIN2* as a reference gene; expression was normalized to that in the wild-type Col-0. Significant differences were tested by Student's *t* test: **$P < 0.01$; *$P < 0.05$; ns, not significant. Error bars represent the SD of three biological replicates for (B and C).
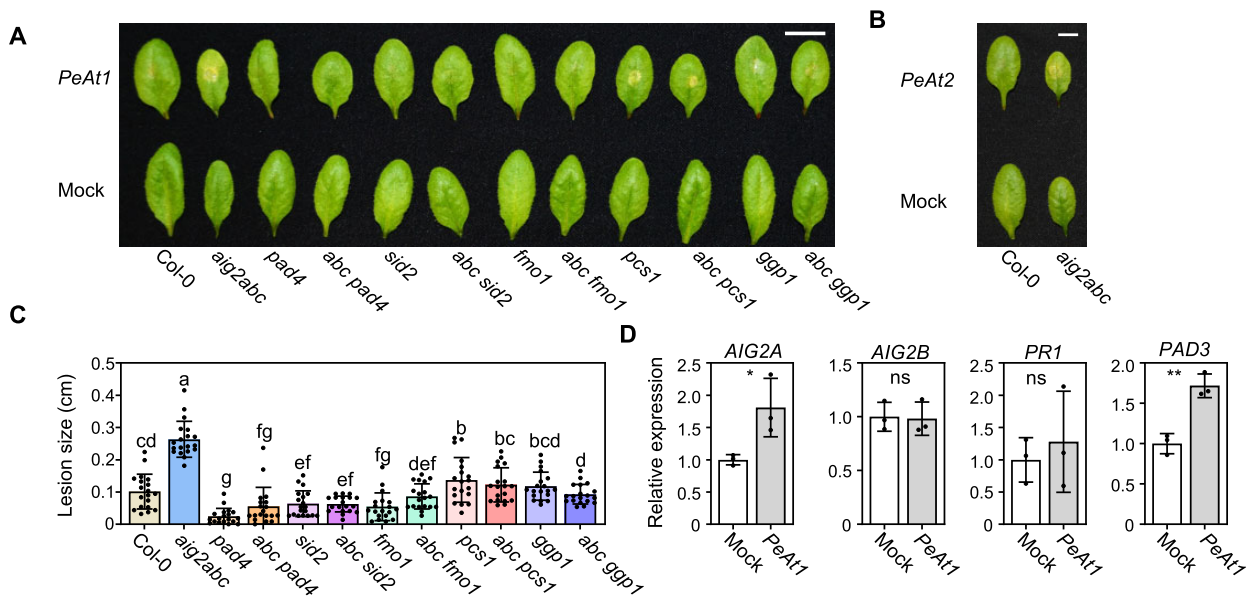
Figure 7 *AIG2*-I genes promote resistance to *Penicillium* sp. in Arabidopsis. A, Resistance phenotypes of Col-0, *aig2abc*, *pad4*, *abc pad4*, *sid2*, *abc sid2*, *fmo1*, *abc fmo1*, *pcs1*, *abc pcs1*, *ggp1*, *abc ggp1*, *79b2 79b3*, and *abc 79b2 79b3* plants to *Penicillium* sp. pv. At1 (*PeAt1*). Shown are the necrotic symptoms of the 5th or 6th true leaf of plants at 7 dpi with *PeAt1*. B, Resistance phenotypes of Col-0 and *aig2abc* to *Penicillium* sp. pv. At2 (*PeAt2*). Shown are the necrotic symptoms of the 5th or 6th true leaves of plants at 7 dpi with *PeAt2*. Scale bars in (A and B), 1 cm. C, Quantification of lesion sizes induced by *PeAt1* in the genotypes in (A). Error bars represent SD from 19 biological replicates. Different letters indicate significant differences ($P < 0.05$) tested by one-way ANOVA with Duncan's post hoc test. D, Expression of *AIG2A*, *AIG2B*, *PR1*, and *PAD3* genes in the wild-type Col-0 at 24 h post-inoculation with *PeAt1*. Shown are relative expression levels analyzed by RT-qPCR using *ACTIN2* as a reference gene; expression was normalized to that in the mock treatment. Error bars represent the SD of three biological replicates. Significant differences were tested by Student's t test: **$P < 0.01$; *$P < 0.05$; ns, not significant.

We further examined the role of the SA-NHP and TDSM defense systems in resistance to *PeAt1*. Mutants of *pad4*, *sid2*, and *fmo1* had smaller lesion sizes and were more resistant to *PeAt1* than the WT (Figure 7C), indicating negative regulation by the SA-NHP system in defense against this fungal pathogen. By contrast, the *pcs1* mutant had a slightly larger lesion size, and the *ggp1* mutant had a slightly increased but not significantly different lesion size compared to the WT (Figure 7C). This suggests that TDSMs play a positive role in resistance to *PeAt1*, but their effect is less pronounced compared to the negative effect of SA-NHP.

Consistent with this hypothesis, mutations in the SA-NHP pathway, including *pad4*, *sid2*, and *fmo1*, reverted the susceptibility to *PeAt1* in the *aig2abc* mutant (Figure 7C). Mutations of *pcs1* or *ggp1* also reduced the susceptibility of the *aig2abc* mutant (Figure 7C), which is consistent with the suppression of the SA-NHP pathway by the TDSM mutations in the *aig2abc* mutant. Therefore, in this interaction with *PeAt1*, *AIG2*-I genes effectively block the upregulation of the SA-NHP system to promote resistance to this fungal pathogen.

AIG2A co-localizes and may interact with TDSM biosynthetic enzymes

Because biosynthetic enzymes of camalexin and other TDSMs were shown to form a metabolic complex in the endoplasmic reticulum (ER; Mucha et al., 2019), we tested whether AIG2A co-localizes with enzymes in TDSM biosynthetic pathways. GFP or mRFP fusions of AIG2A, CYP71A13, GGP1, and PCS1 were transiently expressed in *Nicotiana benthamiana*, and their subcellular localization was examined under a confocal microscope. All of these proteins had very similar localization patterns (Supplemental Figure S12A), suggesting that AIG2A is ER localized. Indeed, CYP71A13-GFP had an overlapping localization signal with ER-mCherry when co-expressed in *N. benthamiana*, consistent with previous findings (Supplemental Figure S12A; Nelson et al., 2007). Interestingly, AIG2A-mRFP, GFP-PCS1, and GGP1-GFP, but not CYP71A13-GFP had additional localization signals in the nucleus (Supplemental Figure S12A). Because nuclear localization has not been reported for PCS1 or GGP1, the validity and function of this observation are yet to be investigated.

We further tested the physical interaction of AIG2A with CYP71A13 and GGP1 by bimolecular fluorescence complementation (BiFC), where proteins were fused to the N-terminus (YFP[N]) or the C-terminus (YFP[C]) of the YFP protein. When YFP[N]-GGP1 and YFP[C]-AIG2A or YFP[N]-CYP71A13 and YFP[C]-AIG2A were co-expressed, positive GFP signals were observed, whereas co-expression of YFP[C]-AIG2A with a fusion protein of YFP[N] and a control protein did not generate positive signals (Supplemental Figure S12B). However, we did not observe positive interactions of AIG2A with CYP71A13, GGP1, or PCS1 in co-IP assays where these proteins tagged with either HA or GFP at their N-termini were transiently co-expressed in *N. benthamiana*. These data

indicate that AIG2A may have a transient or close but not direct physical interaction with the TDSM biosynthetic enzymes GGP1 and CYP71A13.

Putative catalytic residues of AIG2A and AIG2B are required for resistance to *Pst* DC3000

Since AIG2A and AIG2B belong to the psGGCT subfamily of the GGCT superfamily, we determined whether GGCT activity is critical for their function in plant immunity regulation. To this end, we generated mutated forms of AIG2A and AIG2B where the putative catalytic site glutamate at position 83 (E83) was mutated to alanine. The E83 residue is highly conserved in psGGCTs and in other GGCT-like subfamilies, and its corresponding residues E98 in the human GGCT and E82 in the human GGACT have been shown to be essential for their catalytic activities (Figure 8A; Oakley et al., 2008; Oakley et al., 2010). All of the mutated genes were expressed as GFP fusions under their respective native promoters, and the resulting *pAIG2A:AIG2A-E83A:GFP* (*mAIG2A-GFP*) and *pAIG2B:AIG2B-E83A:GFP* (*mAIG2B-GFP*) were transformed into the *aig2abc* mutant (Figure 8, B and C). Neither *mAIG2A-GFP* nor *mAIG2B-GFP* rescued the growth and immunity phenotypes of the *aig2abc* mutant (Figure 8, D and E), despite their proteins accumulating at a similar or even higher level than the wild-type AIG2-GFP proteins (Figure 8C). This suggests that AIG2A and AIG2B likely have a GGCT activity or use the same catalytic site as GGCT for their activity, and that this activity is critical for regulation of disease resistance.

To determine whether AIG2 proteins have GGCT activities toward γ-glutamyl group-containing compounds, we performed an in vitro enzymatic activity assay using recombinant AIG2A-His and AIG2C-His proteins purified from *Escherichia coli* (Supplemental Figure S13A). L-γ-glutamylethylamide (L-theanine) was used as a substrate in the enzymatic reaction because it was shown to be the substrate for a rabbit GGACT (Fink et al, 1980) and it could fit in the substrate pocket of the predicted structure of AIG2A. No GGCT activity on L-theanine was observed for the AIG2A-His protein (Supplemental Figure S13, B–D), but the AIG2C-His protein exhibited some GGCT activity, converting L-theanine to 5-oxo-proline (5-OP) at a detectable amount (Supplemental Figure S13E).

As proteins expressed in *E. coli* may have altered biochemical activities due to the lack of posttranslational modifications that normally occur in plants, we examined the biochemical activities of AIG2A-GFP and AIG2B-GFP fusion proteins purified from transgenic Arabidopsis. With L-theanine as the substrate, no 5-OP, the GGCT product, was detected for AIG2A-GFP or AIG2B-GFP (Supplemental Figure S13, F–G). Considering the possibility that the GGCT activity of AIG2A and AIG2B may require interacting proteins, we further examined the GGCT activity toward L-theanine from the crude total protein extracts from the WT and the *aig2abc* mutant. The abundance of L-theanine was not significantly different between protein extracts from the WT

and the *aig2abc* mutant after L-theanine was added (Supplemental Figure S13H). The 5-OP level was slightly lower (but not significantly different) in the protein extracts from the *aig2abc* mutant compared to in those from the WT with added L-theanine (Supplemental Figure S13H). These data indicate that AIG2A and AIG2B do not have a measurable GGCT activity toward L-theanine, whereas AIG2C might have some GGCT activity.

We also tested whether AIG2A and AIG2B have GGCT activity toward γ-glutamyl-ε-lysine (γ-Glu-ε-Lys), a canonical substrate for human GGACT (Oakley et al., 2010). AIG2A-GFP and AIG2B-GFP proteins purified from transgenic plants did not exhibit enzymatic activity toward this substrate, as determined by the lack of 5-OP product (Supplemental Figure S13I). We also tested GGCT activity using a yeast mutant ABC1723 that is an organic sulfur auxotroph and deficient in GSH utilization (Kumar et al., 2015). This yeast mutant can only grow on medium supplemented with either methionine or cysteine, and therefore a GGCT activity using GSH, γ-glutamyl-cysteine (γ-Glu-Cys) and γ-glutamyl-methionine (γ-Glu-Met) will allow it to grow. As previously reported, the mutant yeast ABC1723 expressing GGCT2;1 was able to grow on medium supplemented with GSH and γ-Glu-Cys, but not with γ-Glu-Met (Supplemental Figure S14A). No growth was found on any of these substrates when the mutant yeast expressed *AIG2A*, *AIG2B*, or *AIG2C*, indicating that AIG2A, AIG2B, and AIG2C do not have a GGCT activity toward these compounds (Supplemental Figure S14A).

In addition, we searched for the AIG2 substrate(s) based on the prediction that it has a glutamyl group and it accumulates to a higher level in the *aig2abc* mutant than in the WT. Glutamyl group-containing compounds characteristically produce m/z 84.04 and m/z 130.05 fragments when analyzed by mass spectrometry (Ma et al., 2013). We applied an untargeted screen for all γ-glutamyl-containing compounds with an MS2 product ion at m/z 84.04 in the WT and the *aig2abc* mutant. Seven such compounds were identified (Supplemental Figure S14, B and C). However, all of them had similar abundances in the *aig2abc* mutant and WT (Supplemental Figure S14, B and C), suggesting that they are not substrates of AIG2A and AIG2B. Therefore, AIG2A and AIG2B may not act on canonical GGCT substrates, and their substrate, as well as the compound that activates the SA-NHP defense pathway, remains elusive.

Discussion

In this study, we established AIG2A and AIG2B as inhibitors of two chemical defense systems in Arabidopsis, acting as gatekeepers to prevent the activation of SA-NHP defense signaling by TDSM defenses, and revealing their biological functions for the first time since these proteins were identified 25 years ago through induction by *Pst* DC3000 (avrRpt2; Reuber and Ausubel, 1996). The AIG2A and AIG2B proteins inhibit SA-NHP defense responses and consequently inhibit resistance to the bacterial pathogen *Pst* DC3000 but
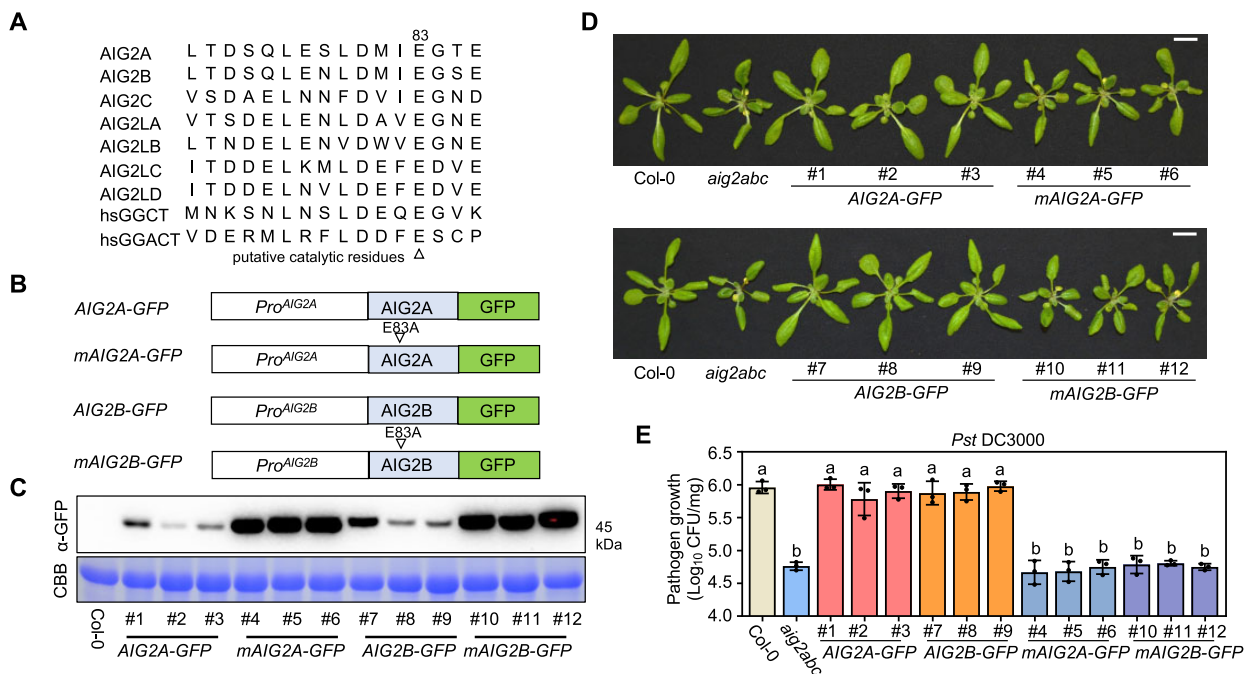
Figure 8 Putative catalytic residues of GGCT are important for AIG2A and AIG2B function. A, Protein sequence alignment of AIG2 homologs in Arabidopsis and human GGCT (hsGGCT) and GGACT (hsGGACT). The sequences near the putative catalytic residue were used. The catalytic residues are indicated by triangles. The protein sequences of hsGGCT (A0A090N7V5) and hsGGACT (Q9BVM4) were retrieved from uniport (https://www.uniprot.org/). B, Schematic diagrams of *pAIG2A:AIG2A:GFP* (*AIG2A-GFP*), *pAIG2A:AIG2A-E83A:GFP* (*mAIG2A-GFP*), *pAIG2B:AIG2B:GFP* (*AIG2B-GFP*), and *pAIG2B:AIG2B-E83A:GFP* (*mAIG2B-GFP*). C, Immunoblot detecting AIG2A-GFP, mAIG2A-GFP, AIG2B-GFP, and mAIG2B-GFP fusion proteins in the transgenic plants by anti-GFP antibodies. CBB, Coomassie brilliant blue. D, Morphology of Col-0, *aig2abc* and three independent lines of *AIG2A-GFP* (#1, #2, and #3), *mAIG2A-GFP* (#4, #5, and #6), *AIG2B-GFP* (#7, #8, and #9), and *mAIG2B-GFP* (#10, #11, and #12) in the *aig2abc* mutant background at 3 weeks old grown under constant light. Scale bar, 1 cm. E, Growth of the bacterial pathogen *Pst* DC3000 in the above genotypes at 3 d post-infection. Error bars represent the SD of three biological replicates. Different letters indicate significant differences ($P < 0.05$) tested by one-way ANOVA with Duncan's post hoc test.

promote resistance to a fungal pathogen in the *Penicillium* genus, where SA plays a negative role (Figures 3 and 7).

More importantly, we revealed the ability of the TDSM chemical defense system to activate the SA-NHP chemical system when the activation is under control of the AIG2A and AIG2B proteins (Figures 5 and 9). The two chemical defense systems were thought to be largely independent, with SA-NHP functioning in resistance to biotrophic pathogens and TDSMs functioning in resistance to necrotrophic fungi, hemibiotrophic fungi, and herbivores (Glazebrook et al., 1997). The only known connection is that SA signaling is important for the biosynthesis of camalexin and indole-3-methylamine (I3A), a breakdown product of IGs (Zhou et al., 1998; Stahl et al., 2016). Here, we provide further evidence that TDSM biosynthesis is largely independent of SA-NHP activation (Figure 5). Neither SA-NHP biosynthesis nor *PAD4*-mediated SA-NHP signaling is required for the induction of TDSM biosynthesis genes in the *aig2abc* mutant (Figure 5). By contrast, genetic and molecular evidence strongly supports that the SA-NHP defense system is activated in a TDSM-dependent manner when AIG2A and AIG2B function is blocked (Figure 5). Knocking out IAOx biosynthetic enzymes, CYP79B2 and CYP79B3, or the GSH conjugate catabolic enzymes, PCS1 or GGP1, which act in

multiple TDSM biosynthetic pathways, inhibits the activation of the SA-NHP pathway in the *aig2abc* mutant (Figure 5). Multiple branches of TDSM biosynthesis are likely required for the full activation of SA-NHP biosynthesis in the *aig2abc* mutant, as mutations in camalexin biosynthesis alone reduced but did not abolish the full expression of SA-NHP biosynthesis genes in the *aig2abc* mutant (Figure 5). AIG2A and AIG2B prevent the activation of SA-NHP chemical defenses by TDSMs. This is likely a critical mechanism to prevent the activation of the SA-NHP pathway when encountering nonpathogenic microbes. Without this safe-guarding mechanism carried out by AIG2A and AIG2B, recognition of nonself signals from nonpathogenic microbes would induce TDSMs that subsequently induce SA-NHP and compromise plant growth. In response to pathogen infection, the AIG2A and AIG2B proteins function to promote resistance when SA-NHP plays a negative role in resistance, such as for the *Penicillium* species (Figure 7). Meanwhile, they could also function as attenuators of defense responses when the SA-NHP system is a key positive player in resistance, as in the case of *Pst* DC3000, to prevent over-activation of the SA-NHP pathway (Figure 6B), which could result in excessive cell death and growth inhibition. AIG2A and AIG2B proteins also function as inhibitors of the
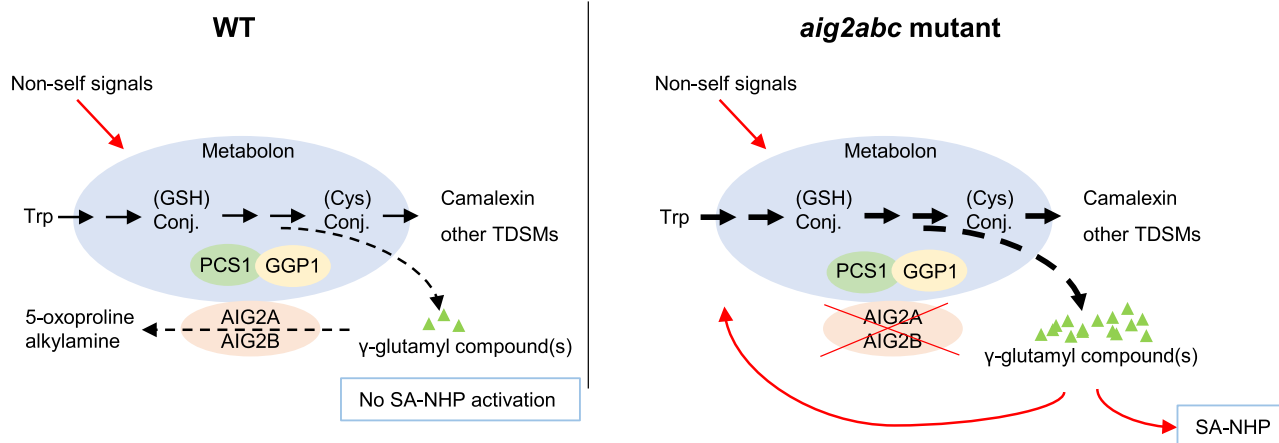
Figure 9 Working model for the role of AIG2A and AIG2B in plant immunity. The Arabidopsis *AIG2A* and *AIG2B* genes encode plant-specific γ-glutamyl cyclotransferases (psGGCT) and are induced by nonself signals and biosynthesis genes of TDSMs. They bind to the metabolon protein complex for biosynthesis of camalexin and potentially other TDSMs to inhibit both TDSM biosynthesis and TDSM-activated SA-NHP biosynthesis. This is likely through their enzymatic activity in converting defense-inducing γ-glutamyl compound(s) to nondefense-inducing compound(s). In the *aig2abc* mutant, the defense-inducing γ-glutamyl compound(s) cannot be metabolized. Nonself signals triggering TDSM biosynthesis are over-activated, resulting in subsequent activation of SA-NHP biosynthesis. The over-activation of SA-NHP biosynthesis represses plant growth and enhances resistance to *Pst* DC3000 but compromises resistance to *Penicillium* pathogens. (GSH)Conj.: glutathione conjugates; (Cys)Conj.: cysteine conjugates; Trp: tryptophan.

TDSM biosynthetic pathways and are themselves co-induced with some TDSM biosynthesis genes (Figure 2, A and B). These characteristics make AIG2A and AIG2B feedback inhibitors that control the extent of TDSM induction by nonself signals (Figure 9). The loss of AIG2A and AIG2B function causes upregulation of TDSM genes under generic lab conditions and in response to pathogen infection but not under sterile conditions (Figure 6, B and C). This suggests that nonself signals induce both TDSM biosynthetic pathways and the expression of *AIG2A* and *AIG2B*, which feedback inhibits TDSM biosynthetic pathways. In addition, induction of AIG2A and AIG2B by PAMPs and pathogen strains is a potential strategy of virulence by *Pst* DC3000, especially because a nonvirulent strain had a minor capability of inducing AIG2A (Supplemental Figure S5B).

The compound(s) from the TDSM biosynthetic pathways that trigger SA and NHP biosynthesis is still unknown. The camalexin pathway alone is not sufficient, as SA-NHP is still upregulated in the *pad3* mutant (Figure 4). Because both PCS1 and GGP1 are required for SA-NHP activation, one or multiple branches of the pathway, including camalexin, ICN, and IG, must play an important role. The intermediates, final products, or byproducts of these TDSM branches may act as a trigger to activate the SA-NHP defense system. Glutamate or glutamate derivates are byproducts of the PCS1 and GGP1 enzymatic reactions, and these compounds have been shown to trigger the immune responses via both SA-dependent and SA-independent mechanisms (Goto et al., 2020). Future studies on products or byproducts of these TDSM pathways as well as a more refined metabolite search may reveal the SA-NHP triggering compound(s).

Our study suggests that AIG2A and AIG2B regulate plant immunity as GGCTs or by enzymatic activity similar to

GGCT. Mutating the putative GGCT catalytic residues abolishes AIG2A and AIG2B functions in immunity (Figure 8). Most GGCT proteins convert γ-glutamyl conjugates into free alkylamine and 5-oxo-L-proline. Therefore, AIG2A and AIG2B might metabolize γ-glutamyl conjugates in the TDSM pathways. AIG2A is co-localized and physically interacts with CYP71A13 and GGP1, which are part of a protein complex (metabolon) for the biosynthesis of camalexin and potentially other TDSMs (Supplemental Figure S12; Mucha et al., 2019). It is possible that the AIG2A and AIG2B proteins convert a γ-glutamyl conjugate, which is able to induce the SA pathway, to a compound that does not have an SA pathway-inducing activity (Figure 9). It is also possible that they may compete with other enzymes for binding to the metabolon to inhibit TDSM biosynthesis. Successful identification of the AIG2A and AIG2B substrates will generate new insights into the activities of both the SA-NHP and the TDSM systems. However, the substrate and biochemical activity of AIG2A and AIG2B remain elusive despite extensive efforts (Supplemental Figures S13 and S14). These Arabidopsis enzymes do not appear to utilize substrates that are common for human GGCTs. Whether or not these plant-specific GGCT members have evolved new enzymatic activities will be interesting to investigate. High-resolution nontargeted metabolomic analysis may be employed in the future to uncover the substrates. This strategy most likely has challenges given the complexity of the different metabolic profiles and general difficulties with analyzing Trp-derived metabolites.

The current study also suggests that expression variation in the *AIG2A* and *AIG2B* genes contributes to variation in resistance to *Pst* DC3000 (Supplemental Figure S1). Most of the *AIG2A* and *AIG2B* polymorphisms that were associated

with resistance to *Pst* DC3000 reside outside of the coding regions, and these polymorphisms are also associated with expression levels of the two genes (Supplemental Figure S4). This genomic region may also have structural variations, which could generate even greater functional variations than gene expression variation. Gene expression variations are known to have a critical role in phenotypic evolution (Wang et al., 2021). It is conceivable that the expression levels of *AIG2A* and *AIG2B* either reflect their inducibility by nonself signals or their capacity to inhibit defense systems in Arabidopsis natural accessions. *AIG2A* and *AIG2B* expression in nature could be shaped by the local microbiome, thereby allowing plants to balance the relative strengths of the TDSM and SA-NHP systems for optimal defense and plant growth. The induction pattern during pathogen infection, which may vary among accessions, could also influence the outcome of plant–pathogen interactions. Therefore, AIG2A and AIG2B likely play a critical role in fine-tuning plant chemical defense systems in a changing environment.

Materials and methods

Plant materials and growth condition
The 100 natural accessions of *A. thaliana* used for GWAS were as described in Wang et al. (2019). Arabidopsis accession Col-0 was the wild type for all mutants in this study. The *pad3-1* and T-DNA insertion mutants SALK_007224 (*aig2c-1*), GABI_319F10 (*ggp1-1*), and SALK_105136 (*cyp71a13*) were obtained from the Arabidopsis Biological Resource Center (ABRC; Alonso et al., 2003; Kleinboelting et al., 2012). Plant materials used in this study are listed in Supplemental Data Set S5. All plants were grown at 22°C under constant light (~100 μmol m^{-2}s^{-1} of cool white fluorescent lamp) and 50% humidity conditions, unless otherwise specified.

Ethyl methanesulfonate mutagenesis and mapping by sequencing
Ethyl methanesulfonate (EMS) mutagenesis was performed as described previously (Yang et al., 2020). In brief, M2 seeds from 10 plants were pooled together, and approximately 800 pools of M2 seeds were screened with approximately 100 plants screened from each pool. Nine WT-like-looking mutants were obtained. The mapping-by-sequencing was carried out as described previously (Hua et al., 2017). Raw sequence reads from Illumina sequencing were mapped to the Arabidopsis TAIR10 genome (https://www.arabidopsis.org/).

RNA-seq and reverse transcription quantitative PCR (RT-qPCR)
For 3' RNA-seq, total RNAs were extracted from whole seedlings of 2-week-old plants using TRIzol reagent (Invitrogen, Cat. No. 15596026) and were purified with the RNA Clean and Concentrator-5 kit (Zymo Research, Cat. No. R1014). Three individual plants were pooled as one biological replicate and three biological replicates were performed. 3' RNA libraries were prepared using a QuantSeq 3' mRNA-Seq Library Prep Kit FWD for Illumina (Lexogen) and were then sequenced on an Illumina NextSeq500 platform, both at the Cornell Genomics Facility. Three biological replicates were performed for each genotype. The raw reads were mapped to the TAIR 10 transcriptome using STAR software (Dobin et al., 2013), with the mismatch limitation set to 1. Differentially expressed genes (DEGs) were identified using the R/edgeR package with the false discovery rate set at ≤0.05 and absolute log base 2 value of fold change (FC) of expression set at ≥1. GO analyses were performed with default settings on the TAIR website (https://www.arabidopsis.org/tools/go_term_enrichment.jsp).

For RT-qPCR, total RNA was extracted from whole seedlings of 2-week-old plants using TRIzol reagent. cDNA was synthesized from 0.5 μg RNA using a PrimeScript RT Reagent Kit with gDNA Eraser (Takara, Cat. No. RR047A). RT-qPCR was performed on a QuantStudio 7 Pro instrument (ThermoFisher Scientific) using iQ SYBR Green supermix (Bio-Rad, Cat. No. 1708880). Three individual plants from one pot were pooled as one biological replicate. At least three biological replicates from different pots were performed. Primers used for RT-qPCR were listed in Supplemental Data Set S6.

Pathogen growth assay
For the *Pst* DC3000 pathogen growth assay, a bacterial suspension (OD600 of 0.05 with 10 mM MgCl$_2$ and 0.02% Silwet L-77) was dip-inoculated on the shoots of 14-d-old plants grown under constant light. Bacterial growth was analyzed at 1 h (0 d) post-inoculation and 3 dpi. The whole shoots of plants were weighed and homogenized in 10 mM MgCl$_2$, and bacteria were counted by plating serial dilutions as described earlier (Yang et al., 2020). Three individual plants from one pot were pooled as one biological replicate. At least three biological replicates from different pots were performed.

Penicillium sp. pv. *At1* (*PeAt1*) and *PeAt2* were isolated and purified from infected leaves of the *aig2abc* mutant and were identified at the Cornell Plant Disease Diagnostic Clinic (plantclinic.cornell.edu). For the *PeAt1* infection assay, 5 μL of spore suspension (5 × 10^6/mL in 0.5 × potato dextrose broth with 0.05% Tween-20) was drop-inoculated on the third pair of true leaves of 4-week-old plants grown under 12-h light/12-h dark conditions. The inoculated plants were covered with a clear plastic dome to keep the humidity high, and disease resistance phenotypes were assayed at 7 dpi. One individual leaf was considered as one biological replicate. Nineteen biological replicates were performed.

Quantification of defense-related metabolites
Quantification of SA was performed exactly as described earlier (Yang et al., 2021). Fifty milligrams of homogenized tissues from 18-d-old seedlings were used. Five biological replicates were performed for each genotype.

For quantification of NHP and camalexin, 18-d-old seedlings were collected and homogenized in liquid nitrogen. To

50 mg homogenized tissues, 2.5 μL of 1 mM [^{15}N]L-glutamic acid (Sigma-Aldrich, Cat. No. 332143-100mg) was added as the internal standard and 250 μL 80% methanol was added to the sample. The mixtures were vortexed and sonicated twice and were then centrifuged at 16,000 × g for 10 mins at room temperature to remove debris. The supernatant was filtered using a 0.22-μM nylon spin filter (Corning, Cat. No. 8169). To 200 μL filtered supernatant, 4 μL of 5.1% formic acid was added and the resulting 10 μL sample was injected into an ExionLC-X500B Q-TOF system for quantification analysis. The LC-MS/MS was operated using the High-Resolution Multiple Reaction Monitoring (MRM-HR) method with a C18 column (Luna C18(2), Phenomenex, 100 mm × 2 mm, i.d. 3 μm). Five biological replicates were performed for each genotype. NHP (MedChemExpress, Cat. No. HY-N7378) and camalexin (Sigma-Aldrich, Cat. No. SML1016) were used as standards for optimization of the MRM method using the guided MRM-HR module in Sciex OS 2.0. The raw data were acquired and processed using Sciex OS 2.0 software and the relative quantitation of NHP and camalexin was carried out by integrating the peak areas of each analyte using MRM-HR transitions after normalization against the internal standard. Six individual plants from one pot were pooled as one biological replicate. At least four biological replicates from different pots were performed.

GWAS

Four-week-old plants grown under 12-h light/12-h dark conditions were spray-inoculated with a *Pst* DC3000 (OD600 of 0.05) bacteria suspension. Bacterial growth was analyzed at 1 h post-inoculation (0 dpi) and 3 dpi. Three biological replicates for each accession were performed. The difference between 3 dpi and 0 dpi of each accession was used as disease resistance phenotype input. GWAS was performed on GWAPP (https://gwapp.gmi.oeaw.ac.at/index.html) with a 250 K single-nucleotide polymorphism (SNP) dataset (Seren et al., 2012). The accelerated mixed model method was used, and the minor allele count (MAC) was set to 15 to remove minor SNPs for the GWA result.

The eGWAS of 665 natural accessions was performed on the GWA-Portal website with 10 M SNPs from the 1,135 SNP dataset (Alonso-Blanco et al., 2016). The read counts of genes extracted from the processed RNA-Seq count data (Kawakatsu et al., 2016) were used for eGWAS without transformation. The accelerated mixed model method was used, and MAC was set to 34.

Phylogenetic analysis

For the Arabidopsis homolog search, the AIG2A protein sequence was used as a query in a BLASTp search (https://blast.ncbi.nlm.nih.gov/) against the Arabidopsis UniProtKB/Swiss-Prot (swissprot) protein database, with expected threshold set at 1E-15. The resulting sequences were aligned using the MUSCLE algorithm with default parameters (Gap Open, −2.90; Gap Extend, 0.00; Hydrophobicity Multiplier, 1.20) and were subsequently used for phylogenetic analysis

(Supplemental File S1). An unrooted maximum likelihood tree was built with all amino acid sequences using MEGA-X software (Supplemental File S2; Kumar et al., 2018).

Plasmid construction and transgenic plant generation

For genome editing, the target sequences in AIG2 family genes were identified using CRISPR-P 2.0 (http://crispr.hzau.edu.cn/CRISPR2/). CRISPR/Cas9 constructs were generated in the pHEE401E vector (Wang et al., 2015).

For complementation analyses, a genomic fragment of *AIG2A* (from 1.8 kb 5′ of translation initiation site [TIS] to 300 bp 3′ to translation termination site [TTS]), a genomic fragment of *AIG2B* (from 1 kb 5′ TIS to 800 bp 3′ TTS), a genomic fragment of *AIG2C* (from 700 bp TIS to 400 bp 3′ TTS), a genomic fragment of *GGP1* (from 2 kb 5′ TIS to 1 kb 3′ TTS), and a genomic fragment of *PCS1* (from 1.4 kb 5′ TIS to 1.1 kb 3′ TTS) were amplified by PCR and were cloned into the pCR8/GW/TOPO vector (Invitrogen, Cat. No. K250020). These fragments were recombined into the binary vector pMDC99 (Curtis and Grossniklaus, 2003) using Gateway LR Clonase (Invitrogen, Cat. No. 11791-020).

For *pAIG2A:AIG2A:GFP* and *pAIG2B:AIG2B:GFP* construction, genomic fragments of *AIG2A* (from 1 kb 5′ TIS to TTS, without TTS) and *AIG2B* (from 1 kb 5′ TIS to TTS, without TTS) were amplified by PCR and were cloned into the pDONOR222 entry vector using Gateway BP Clonase (Invitrogen, Cat. No. 11789020). For *pAIG2A:AIG2A-E83A:GFP* and *pAIG2B:AIG2B-E83A:GFP* construction, the mutations were introduced into *pAIG2A:AIG2A:GFP* and *pAIG2B:AIG2B:GFP* entry vectors by PCR amplification and the ClonExpress II One Step Cloning kit (Vazyme, Cat. No. C112), respectively. These fragments were then recombined into the binary vector pGWB540 (Nakagawa et al., 2007).

For generating constructs for co-localization and bimolecular fluorescence complementation (BiFC) assays, the genomic fragments of *CYP71A13* (from TIS to TSS, without TSS) and *GGP1* (from TIS to TSS, without TSS) were amplified by PCR and were cloned into the pDONOR222 entry vector. These fragments were then recombined into the binary vector pGWB551 to generate *35S:CYP71A13:GFP* and *35S:GGP1:GFP* constructs or into pSPYNE-35SGW and pSPYCE-35SGW (Walter et al., 2004) to generate *35S:CYP71A13:YFP^N*, *35S:CYP71A13:YFP^C*, *35S:GGP1:YFP^N* and *35S:GGP1:YFP^C* constructs. The genomic fragment of *AIG2A* (from TIS to TSS, without TSS) was amplified by PCR and was cloned into pCR8/GW/TOPO and was then recombined into pSPYCE-35SGW to generate the *35S:AIG2A:YFP^C* construct. The genomic fragment of *PCS1* (from TIS to TSS) was introduced into pCR8/GW/TOPO and was then recombined into the pMDC43 vector to generate the *35S:GFP:PCS1* construct. The genomic fragment of *AIG2A* (from TIS to TSS, without TSS) and coding sequence of mRFP amplified from the pGWB553 vector were fused by PCR, and the resulting fragment was cloned into pDNOR222 and was then

recombined into the pGWB402 vector to generate *35S:AIG2A:mRFP* construct.

For *AIG2A-His*, *AIG2C-His* construction, the cDNA fragments of *AIG2A* and *AIG2C* were PCR amplified from a Col-0 cDNA library. The fragments were digested with *Nhe*I and *Bam*HI restriction enzymes and ligated into the pKS-His vector using T4 DNA ligase (NEB, Cat. No. M0202L). *Escherichia coli* strain BL21(DE3) was used for expressing the recombined proteins.

For generating constructs for the enzymatic activity assay in *Saccharomyces cerevisiae*, the cDNA fragments of *AIG2A*, *AIG2B*, *AIG2C*, and *GGCT2;1* were PCR amplified from a Col-0 cDNA library. The fragments were digested with *Bam*HI and *Xho*I restriction enzymes and ligated into the p416TEF vector using T4 DNA ligase. *Saccharomyces cerevisiae* strain ABC1723 (*MATα his3Δ1 leu2Δ0 lys2Δ0 met15Δ0 ura3Δ0 ecm38Δ::KanMX4 dug3*) was used for the in vivo enzymatic activity assay.

Primers used for plasmid construction are listed in Supplemental Data Set S6. *Agrobacterium tumefaciens* strain GV3101 (pMP90) carrying the desired construct was used for floral dipping to generate transgenic plants or for transient expression in *N. benthamiana*.

Immunoblotting

Total protein was extracted from 2-week-old plants grown under 12-h light/12-h dark conditions. The GFP fusion proteins were detected with anti-GFP antibody (Takara, Cat. No. 632381, at a 1:3,000 dilution) and an HRP-linked secondary antibody (Cell Signaling, Cat. No. 7076, at a 1:5,000 dilution). Membranes were photographed with the Bio-Rad ChemiDoc imaging system.

Purification of recombinant protein from *E. coli* and Arabidopsis

To produce AIG2A-His and AIG2C-His in *E. coli*, the corresponding BL21 strains were inoculated into 5 mL liquid LB medium supplemented with 100 μg/mL carbenicillin and grown overnight at 37°C. A 500-μL aliquot from each culture was used to inoculate 50 mL of LB medium supplemented with 100 μg/mL carbenicillin at 37°C. Once the OD600 reached 0.8, 0.25 mM isopropyl β-D-1-thiogalactopyranoside (IPTG) was added into the media, and the media were shaken at 20°C for another 3 h. The cells were pelleted and collected by centrifuging at $6,000 \times g$ for 10 min at 4°C. The His-tagged proteins were purified using Ni-NTA agarose (Qiagen, Cat. No. 30210) according to the manufacturer's instruction. The concentration of purified proteins was quantified with a Bradford assay.

To isolate recombinant proteins from Arabidopsis, proteins were extracted with 4 mL Tris-buffered saline (TBS; 50 mM Tris-HCl, pH 7.5, 150 mM NaCl, 1 mM EDTA, 0.25% Triton-X100, 1 mM PMSF, 1% protease inhibitor cocktail, Sigma, Cat. No. P9599) from 1 g tissues of *pAIG2A:AIG2A:GFP* and *pAIG2B:AIG2B:GFP* transgenic plants. The AIG2A-GFP and AIG2B-GFP proteins were purified with GFP-Trap Magnetic Agarose (Chromotek, Cat. No. gtma-10) according to the manufacturer's instructions.

In vitro enzymatic activity assay

The AIG2A-His and AIG2C-His proteins were dialyzed in 20 mM Tris-HCl (pH 8.0) and 0.1 mM dithiothreitol (DTT) at 4°C for 1 h and concentrated to ~2.5 mg/mL prior to use. A 200-μL standard enzyme reaction mixture contained 20 μL of 1 M Tris-HCl (pH 8.0), 20 μL 2 mM γ-Glu-ε-Lys or 20 μL 150 mM L-theanine, 5 μL enzymes, and 15 μL AIG2A-GFP or AIG2B-GFP bound beads. The reactions were initiated by adding the enzymes, incubated at room temperature for 1 h, and then quenched by adding 200 μL 10% acetic acid. For in vitro enzymatic activity assays with crude protein extracts, crude proteins were extracted with 100 mM Tris-HCl (pH 8.0) from Col-0 or the *aig2abc* mutant plants. L-theanine (10 μL, 150 mM) was mixed with 90 μL crude protein extracts, incubated at room temperature for 1 h, and then quenched by adding 100 μL 10% acetic acid.

Quenched reactions were centrifuged at $14,000 \times g$ for 2 min at 4°C to remove protein or beads. L-glutamic acid-^{15}N (200 μL, 0.25 mM) in 100% methanol was added to 50 μL of supernatant. The mixtures were vortexed and sonicated twice and were then centrifuged at $16,000 \times g$ for 10 min at 22°C to remove the debris. To 200 μL filtered supernatant, 4 μL of 5.1% formic acid was added and the resulting 10 μL of sample was injected into the ExionLC-X500B Q-TOF Sciex system for targeted quantification analysis. The LC-MS/MS was operated on a positive ionization mode using a High-Resolution Multiple Reaction Monitoring (MRM-HR) method with a C18 column (Luna C18(2), Phenomenex, 100 mm × 2 mm, i.d. 3 μm) for gradient elution using buffer A (0.1% formic acid in water) and buffer B (0.1% formic acid and 95% acetonitrile in water). γ-Glu-ε-Lys (MedChemExpress, Cat. No. HY-113089), L-theanine (Cayman, Cat. No. 20832), and 5-oxo-proline (Sigma-Aldrich, Cat. No. 83160) were used as standards for optimization of the MRM method using the guided MRM-HR module in Sciex OS 2.0. The raw data were acquired and processed using Sciex OS 2.0 software and the relative quantitation of γ-Glu-ε-Lys, L-theanine, and 5-oxo-proline was carried out by integrating the peak areas of each analyte using MRM-HR transitions after normalization against the internal standard.

Screening for compounds containing a glutamyl group

To 50 mg homogenized tissues, 2.5 μL of 1 mM L-glutamic acid-^{15}N was added as the internal standard and 250 μL of 80% methanol was added to the sample. The mixtures were vortexed and sonicated twice and were then centrifuged at $16,000 \times g$ for 10 min at room temperature to remove the debris. The supernatant was filtered using a 0.22-μM nylon spin filter. To 200 μL of filtered supernatant, 4 μL of 5.1% formic acid was added and the resulting 10 μL of sample was injected into an Orbitrap Fusion mass spectrometer coupled with a UHPLC Ultimate 3000 system with the same C18 column (Luna C18(2), Phenomenex, 100 mm × 2 mm,

i.d. 3 μm) as that used for gradient elution, using buffer A (0.1% formic acid in water) and buffer B (0.1% formic acid and 95% acetonitrile in water). For mass analysis, the analytes with a product ion at m/z 84.0444 triggered additional MS/MS2 DDA for the targeted precursor ions, intending to identify only the compounds having a glutamyl group as one of the major fragments. Six individual plants from one pot were pooled as one biological replicate. Three biological replicates were performed for each genotype. The raw data were acquired and processed using Xcalibur 3.3 software and the peak area of each of the ions was measured.

Statistical analysis

Student's *t* tests were performed using Excel. One-way analysis of variation (ANOVA) followed by Duncan's new multiple range tests was performed using R 3.6.3 with the "agricolae" package (https://cran.r-project.org/web/packages/agricolae/). Statistical tests and biological replicate numbers are described in the figure legends or methods. Detailed statistical results are provided in Supplemental Data Set S7.

Accession numbers

DNA sequences of all genes in this study were extracted from The Arabidopsis Information Resource (TAIR, https://www.arabidopsis.org/) with the following gene IDs: *AIG2A* (AT3G28930); *AIG2B* (AT3G28940); *AIG2C* (AT3G28950); *AIG2LA* (AT5G39720); *AIG2LB* (AT5G39730); *AIG2LC* (AT4G31310); *AIG2LD* (AT2G24390); *SID2* (AT1G74710); *CAMTA3* (AT2G22300); *PCS1* (AT5G44070); *GGP1* (AT4G30530); *ACTIN2* (AT3G18780); *PAD3* (AT3G26830); *CYP71A13* (AT2G30770); *CBP60g* (AT5G26920); *SARD1* (AT1G73805); *SARD4* (AT5G52810); *FMO1* (AT1G19250); *PAD4* (AT3G52430); *EDS1* (AT3G48090); *PR1* (AT2G14610); *FOX1* (AT1G26380); *CYP81F2* (AT5G57220); *CYP79B2* (AT4G39950); *CYP79B3* (AT2G22330).

RNA-seq data of this study can be found at NCBI GEO under the accession number GSE196599.

Supplemental data

The following materials are available in the online version of this article.

Supplemental Figure S1. GWAS of resistance to *Pst* DC3000 in Arabidopsis natural accessions (supports Figure 1).

Supplemental Figure S2. Characterization of mutants generated in the *AIG2* genes (supports Figure 1).

Supplemental Figure S3. Loss of AIG2A and AIG2B function confers enhanced resistance to *Pst* DC3000 (supports Figure 1).

Supplemental Figure S4. Expression GWAS of *AIG2A* and *AIG2B* expression in Arabidopsis (supports Figure 1).

Supplemental Figure S5. *AIG2*-I genes are induced by biotic stresses (supports Figure 2).

Supplemental Figure S6. Characterization of mutants identified from suppressor screens (supports Figures 3 and 4).

Supplemental Figure S7. GO analysis of DEGs in the *aig2abc* mutant versus the wild type (supports Figure 5).

Supplemental Figure S8. *AIG2*-I genes repressed expression of biosynthesis genes in SA-NHP and TDSM systems (supports Figure 5).

Supplemental Figure S9. *AIG2*-I genes are co-expressed with Trp and TDSM biosynthesis genes (supports Figure 5).

Supplemental Figure S10. GO analysis of upregulated DEGs in the *aig2abc pad4* mutant versus the *pad4* mutant (supports Figure 5).

Supplemental Figure S11. The *aig2abc* mutant did not exhibit a different level of resistance to *Botrytis cinerea* or *Alternaria brassicicola* compared to the wild type (supports Figure 7).

Supplemental Figure S12. AIG2A co-localizes and physically interacts with TDSM biosynthetic enzymes (supports Figure 5).

Supplemental Figure S13. AIG2A and AIG2B do not exhibit GGCT activity toward L-theanine and γ-glutamyl-ε-Lysine (γ-Glu-ε-Lys; supports Figure 8).

Supplemental Figure S14. AIG2A and AIG2B do not exhibit GGCT activity toward GSH, γ-glutamyl-cysteine (γ-Glu-Cys), and γ-glutamyl-methionine (γ-Glu-Met; supports Figure 8).

Supplemental Data Set S1. Analysis of resistance to *Pseudomonas syringae* pv. *tomato* (*Pst*) DC3000 in Arabidopsis natural accessions.

Supplemental Data Set S2. Co-expressed genes of *AIG2A*.

Supplemental Data Set S3. DEGs in the *aig2abc* mutant compared to the wild-type Col-0.

Supplemental Data Set S4. DEGs in the *aig2abc pad4* mutant compared to the *pad4* mutant.

Supplemental Data Set S5. Plant materials used in this study.

Supplemental Data Set S6. Primers used in this study.

Supplemental Data Set S7. Summary of statistical analyses.

Supplemental File S1. Sequence alignment file for Figure 1A.

Supplemental File S2. Tree file for Figure 1A.

Conflict of Interest statement. The authors declare no conflicts of interest.

References

Aerts N, Pereira Mendes M, Van Wees SC (2021) Multiple levels of crosstalk in hormone networks regulating plant defense. Plant J **105**: 489–504

Agerbirk N, De Vos M, Kim JH, Jander G (2009) Indole glucosinolate breakdown and its biological effects. Phytochem Rev **8**: 101–120

Alonso JM, Stepanova AN, Leisse TJ, Kim CJ, Chen H, Shinn P, Stevenson DK, Zimmerman J, Barajas P, Cheuk R, et al. (2003) Genome-wide insertional mutagenesis of *Arabidopsis thaliana*. Science **301**:653–657

Alonso-Blanco C, Andrade J, Becker C, Bemm F, Bergelson J, Borgwardt KM, Cao J, Chae E, Dezwaan TM, Ding W, et al. (2016) 1,135 genomes reveal the global pattern of polymorphism in *Arabidopsis thaliana*. Cell **166**: 481–491

Bauer S, Mekonnen DW, Hartmann M, Yildiz I, Janowski R, Lange B, Geist B, Zeier J, Schäffner AR (2021) UGT76B1, a promiscuous hub of small molecule-based immune signaling, glucosylates N-hydroxypipecolic acid, and balances plant immunity. Plant Cell **33**: 714–734

Bjornson M, Pimprikar P, Nürnberger T, Zipfel C (2021) The transcriptional landscape of Arabidopsis thaliana pattern-triggered immunity. Nat Plants **7**: 579–586

Chen YC, Holmes EC, Rajniak J, Kim JG, Tang S, Fischer CR, Mudgett MB, Sattely ES (2018) N-hydroxy-pipecolic acid is a mobile metabolite that induces systemic disease resistance in Arabidopsis. Proc Natl Acad Sci USA **115**: E4920–E4929

Clay NK, Adio AM, Denoux C, Jander G, Ausubel FM (2009) Glucosinolate metabolites required for an Arabidopsis innate immune response. Science **323**: 95–101

Curtis MD, Grossniklaus U (2003) A gateway cloning vector set for high-throughput functional analysis of genes in planta. Plant Physiol **133**: 462–469

Ding P, Rekhter D, Ding Y, Feussner K, Busta L, Haroth S, Xu S, Li X, Jetter R, Feussner I, et al. (2016) Characterization of a pipecolic acid biosynthesis pathway required for systemic acquired resistance. Plant Cell **28**: 2603–2615

Ding Y, Sun T, Ao K, Peng Y, Zhang Y, Li X, Zhang Y (2018) Opposite roles of salicylic acid receptors NPR1 and NPR3/NPR4 in transcriptional regulation of plant immunity. Cell **173**: 1454–1467

Dobin A, Davis CA, Schlesinger F, Drenkow J, Zaleski C, Jha S, Batut P, Chaisson M, Gingeras TR (2013) STAR: ultrafast universal RNA-seq aligner. Bioinformatics **29**: 15–21

Ferrari S, Plotnikova JM, De Lorenzo G, Ausubel FM (2003) Arabidopsis local resistance to *Botrytis cinerea* involves salicylic acid and camalexin and requires *EDS4* and *PAD2*, but not *SID2*, *EDS5* or *PAD4*. Plant J **35**: 193–205

Fink ML, Chung SI, Folk JE (1980) γ-Glutamylamine cyclotransferase: specificity toward ε-(L-γ-glutamyl)-L-lysine and related compounds. Proc Natl Acad Sci USA **77**: 4564–4568

Glazebrook J, Rogers EE, Ausubel FM (1997) Use of Arabidopsis for genetic dissection of plant defense responses. Annu Rev Genet **31**: 547–569

Geu-Flores F, Nielsen MT, Nafisi M, Møldrup ME, Olsen CE, Motawia MS, Halkier BA (2009) Glucosinolate engineering identifies a γ-glutamyl peptidase. Nat Chem Biol **5**: 575–577

Geu-Flores F, Møldrup ME, Böttcher C, Olsen CE, Scheel D, Halkier BA (2011) Cytosolic γ-glutamyl peptidases process glutathione conjugates in the biosynthesis of glucosinolates and camalexin in Arabidopsis. Plant Cell **23**: 2456–2469

Glawischnig E (2007) Camalexin. Phytochemistry **68**: 401–406

Goto Y, Maki N, Ichihashi Y, Kitazawa D, Igarashi D, Kadota Y, Shirasu K (2020) Exogenous treatment with glutamate induces immune responses in Arabidopsis. Mol Plant Microbe Interact **33**: 474–487

Hartmann M, Kim D, Bernsdorff F, Ajami-Rashidi Z, Scholten N, Schreiber S, Zeier T, Schuck S, Reichel-Deland V, Zeier J (2017) Biochemical principles and functional aspects of pipecolic acid biosynthesis in plant immunity. Plant Physiol **174**: 124–153

Hartmann M, Zeier T, Bernsdorff F, Reichel-Deland V, Kim D, Hohmann M, Scholten N, Schuck S, Bräutigam A, Hölzel T, et al (2018) Flavin monooxygenase-generated N-hydroxypipecolic acid is a critical element of plant systemic immunity. Cell **173**: 456–469

Hématy K, Lim M, Cherk C, Piślewska-Bednarek M, Sanchez-Rodriguez C, Stein M, Fuchs R, Klapprodt C, Lipka V, Molina A, et al. (2020) Moonlighting function of phytochelatin synthase1 in extracellular defense against fungal pathogens. Plant Physiol **182**: 1920–1932

Hiruma K, Fukunaga S, Bednarek P, Piślewska-Bednarek M, Watanabe S, Narusaka Y, Shirasu K, Takano Y (2013) Glutathione and tryptophan metabolism are required for Arabidopsis immunity during the hypersensitive response to hemibiotrophs. Proc Natl Acad Sci USA **110**: 9589–9594

Hua J (2013) Modulation of plant immunity by light, circadian rhythm, and temperature. Curr Opin Plant Biol **16**: 406–413

Hua J, Wang S, Sun Q (2017) Mapping and cloning of chemical induced mutations by whole-genome sequencing of bulked segregants. *In* Plant pattern recognition receptors. Humana Press, New York, NY, pp 285–289.

Huang J, Gu M, Lai Z, Fan B, Shi K, Zhou YH, Yu JQ, Chen Z (2010) Functional analysis of the Arabidopsis *PAL* gene family in plant growth, development, and response to environmental stress. Plant Physiol **153**: 1526–1538

Huang W, Wang Y, Li X, Zhang Y (2020) Biosynthesis and regulation of salicylic acid and N-hydroxypipecolic acid in plant immunity. Mol Plant **13**: 31–41

Jing B, Xu S, Xu M, Li Y, Li S, Ding J, Zhang Y (2011) Brush and spray: a high-throughput systemic acquired resistance assay suitable for large-scale genetic screening. Plant Physiol **157**: 973–980

Jirage D, Tootle TL, Reuber TL, Frost LN, Feys BJ, Parker JE, Ausubel FM, Glazebrook J (1999) Arabidopsis thaliana PAD4 encodes a lipase-like gene that is important for salicylic acid signaling. Proc Natl Acad Sci USA **96**: 13583–13588

Joshi NC, Meyer AJ, Bangash SA, Zheng ZL, Leustek T (2019) Arabidopsis γ-glutamylcyclotransferase affects glutathione content and root system architecture during sulfur starvation. New Phytol **221**: 1387–1397

Kawakatsu T, Huang SSC, Jupe F, Sasaki E, Schmitz RJ, Urich MA, Castanon R, Nery JR, Barragan C, He Y, et al. (2016) Epigenomic diversity in a global collection of Arabidopsis thaliana accessions. Cell **166**: 492–505

Kleinboelting N, Huep G, Kloetgen A, Viehoever P, Weisshaar B (2012) GABI-Kat SimpleSearch: new features of the Arabidopsis thaliana T-DNA mutant database. Nucleic Acids Res **40**: D1211–D1215

Kumar S, Kaur A, Chattopadhyay B, Bachhawat AK (2015) Defining the cytosolic pathway of glutathione degradation in Arabidopsis thaliana: role of the ChaC/GCG family of γ-glutamyl cyclotransferases as glutathione-degrading enzymes and AtLAP1 as the Cys-Gly peptidase. Biochem J **468**: 73–85

Kumar S, Stecher G, Li M, Knyaz C, Tamura K (2018) MEGA X: molecular evolutionary genetics analysis across computing platforms. Mol Biol Evol **35**: 1547.

Liu Y, Sun T, Sun Y, Zhang Y, Radojičić A, Ding Y, Tian H, Huang X, Lan J, Chen S, et al. (2020) Diverse roles of the salicylic acid receptors NPR1 and NPR3/NPR4 in plant immunity. Plant Cell **32**: 4002–4016

Ma X, Dagan S, Somogyi Á, Wysocki VH, Scaraffia PY (2013) Low mass MS/MS fragments of protonated amino acids used for

distinction of their 13C-isotopomers in metabolic studies. J Am Soc Mass Spectrom **24**: 622–631

Maier BA, Kiefer P, Field CM, Hemmerle L, Bortfeld-Miller M, Emmenegger B, Schäfer M, Pfeilmeier S, Sunagawa S, Vogel CM, et al. (2021) A general non-self response as part of plant immunity. Nat Plants **7**: 696–705

Mine A, Seyfferth C, Kracher B, Berens ML, Becker D, Tsuda K (2018) The defense phytohormone signaling network enables rapid, high-amplitude transcriptional reprogramming during effector-triggered immunity. Plant Cell **30**: 1199–1219

Mikkelsen MD, Hansen CH, Wittstock U, Halkier BA (2000) Cytochrome P450 CYP79B2 from Arabidopsis catalyzes the conversion of tryptophan to indole-3-acetaldoxime, a precursor of indole glucosinolates and indole-3-acetic acid. J Biol Chem **275**: 33741–33717

Mucha S, Heinzlmeir S, Kriechbaumer V, Strickland B, Kirchhelle C, Choudhary M, Kowalski N, Eichmann R, Hückelhoven R, Grill E, et al. (2019) The formation of a camalexin biosynthetic metabolon. Plant Cell **31**: 2697–2710

Müller TM, Böttcher C, Glawischnig E (2019) Dissection of the network of indolic defence compounds in *Arabidopsis thaliana* by multiple mutant analysis. Phytochemistry **161**: 11–20

Møldrup ME, Geu-Flores F, Halkier BA (2013) Assigning gene function in biosynthetic pathways: camalexin and beyond. Plant Cell **25**: 360–367

Nafisi M, Goregaoker S, Botanga CJ, Glawischnig E, Olsen CE, Halkier BA, Glazebrook J (2007) Arabidopsis cytochrome P450 monooxygenase 71A13 catalyzes the conversion of indole-3-acetaldoxime in camalexin synthesis. Plant Cell **19**: 2039–2052

Nakagawa T, Suzuki T, Murata S, Nakamura S, Hino T, Maeo K, Tabata R, Kawai T, Tanaka K, Niwa Y, et al. (2007) Improved Gateway binary vectors: high-performance vectors for creation of fusion constructs in transgenic analysis of plants. Biosci Biotechnol Biochem **71**: 2095–2100

Nawrath C, Métraux JP (1999) Salicylic acid induction–deficient mutants of Arabidopsis express PR-2 and PR-5 and accumulate high levels of camalexin after pathogen inoculation. Plant Cell **11**: 1393–1404

Nelson BK, Cai X, Nebenführ A (2007) A multicolored set of in vivo organelle markers for co-localization studies in Arabidopsis and other plants. Plant J **51**: 1126–1136

Nie H, Zhao C, Wu G, Wu Y, Chen Y, Tang D (2012) SR1, a calmodulin-binding transcription factor, modulates plant defense and ethylene-induced senescence by directly regulating *NDR1* and *EIN3*. Plant Physiol **158**: 1847–1859

Oakley AJ, Coggan M, Board PG (2010) Identification and characterization of γ-glutamylamine cyclotransferase, an enzyme responsible for γ-glutamyl-∊-lysine catabolism. J Biol Chem **285**: 9642–9648

Oakley AJ, Yamada T, Liu D, Coggan M, Clark AG, Board PG (2008) The identification and structural characterization of C7orf24 as γ-glutamyl cyclotransferase: an essential enzyme in the γ-glutamyl cycle. J Biol Chem **283**: 22031–22042

Pastorczyk M, Bednarek P (2016) The function of glucosinolates and related metabolites in plant innate immunity. Adv Bot Res **80**: 171–198

Pastorczyk M, Kosaka A, Piślewska-Bednarek M, López G, Frerigmann H, Kułak K, Glawischnig E, Molina A, Takano Y, Bednarek P (2020) The role of CYP71A12 monooxygenase in pathogen-triggered tryptophan metabolism and Arabidopsis immunity. New Phytol **225**: 400–412

Paasch BC, He SY (2021) Toward understanding microbiota homeostasis in the plant kingdom. PLoS Pathog **17**: e1009472

Paulose B, Chhikara S, Coomey J, Jung HI, Vatamaniuk O, Dhankher OP (2013) A γ-glutamyl cyclotransferase protects Arabidopsis plants from heavy metal toxicity by recycling glutamate to maintain glutathione homeostasis. Plant Cell **25**: 4580–4595

Rajniak J, Barco B, Clay NK, Sattely ES (2015) A new cyanogenic metabolite in Arabidopsis required for inducible pathogen defence. Nature **525**: 376–379

Rekhter D, Lüdke D, Ding Y, Feussner K, Zienkiewicz K, Lipka V, Wiermer M, Zhang Y, Feussner I (2019) Isochorismate-derived biosynthesis of the plant stress hormone salicylic acid. Science **365**: 498–502

Reuber TL, Ausubel FM (1996) Isolation of Arabidopsis genes that differentiate between resistance responses mediated by the RPS2 and RPM1 disease resistance genes. Plant Cell **8**: 241–249

Seren Ü, Vilhjálmsson BJ, Horton MW, Meng D, Forai P, Huang YS, Long Q, Segura V, Nordborg M (2012) GWAPP: a web application for genome-wide association mapping in Arabidopsis. Plant Cell **24**: 4793–4805

Stahl E, Bellwon P, Huber S, Schlaeppi K, Bernsdorff F, Vallat-Michel A, Mauch F, Zeier J (2016) Regulatory and functional aspects of indolic metabolism in plant systemic acquired resistance. Mol Plant **9**: 662–681

Sun T, Huang J, Xu Y, Verma V, Jing B, Sun Y, Orduna AR, Tian H, Huang X, Xia S, et al. (2020) Redundant CAMTA transcription factors negatively regulate the biosynthesis of salicylic acid and N-hydroxypipecolic acid by modulating the expression of *SARD1* and *CBP60g*. Mol Plant **13**: 144–156

Thomma BP, Nelissen I, Eggermont K, Broekaert WF (1999) Deficiency in phytoalexin production causes enhanced susceptibility of *Arabidopsis thaliana* to the fungus *Alternaria brassicicola*. Plant J **19**: 163–171

Torrens-Spence MP, Bobokalonova A, Carballo V, Glinkerman CM, Pluskal T, Shen A, Weng JK (2019) PBS3 and EPS1 complete salicylic acid biosynthesis from isochorismate in Arabidopsis. Mol Plant **12**: 1577–1586

Vlot AC, Dempsey DMA, Klessig DF (2009) Salicylic acid, a multifaceted hormone to combat disease. Annu Rev Phytopathol **47**: 177–206

Wan WL, Kim ST, Castel B, Charoennit N, Chae E (2021) Genetics of autoimmunity in plants: an evolutionary genetics perspective. New Phytol **229**: 1215–1233

Wang L, Tsuda K, Truman W, Sato M, Nguyen LV, Katagiri F, Glazebrook J (2011) CBP60g and SARD1 play partially redundant critical roles in salicylic acid signaling. Plant J **67**: 1029–1041

Wang Z, Yang L, Liu Z, Lu M, Wang M, Sun Q, Lan Y, Shi T, Wu D, Hua J (2019) Natural variations of growth thermo-responsiveness determined by SAUR26/27/28 proteins in *Arabidopsis thaliana*. New Phytol **224**: 291–305

Wang Z, Yang L, Wu D, Zhang N, Hua J (2021) Polymorphisms in cis-elements confer *SAUR26* gene expression difference for thermo-response natural variation in Arabidopsis. New Phytol **229**: 2751–2764

Wang ZP, Xing HL, Dong L, Zhang HY, Han CY, Wang XC, Chen QJ (2015) Egg cell-specific promoter-controlled CRISPR/Cas9 efficiently generates homozygous mutants for multiple target genes in Arabidopsis in a single generation. Genome Biol **16**: 1–12

Wagner U, Edwards R, Dixon DP, Mauch F (2002) Probing the diversity of the Arabidopsis glutathione S-transferase gene family. Plant Mol Biol **49**: 515–532

Walter M, Chaban C, Schütze K, Batistic O, Weckermann K, Näke C, Blazevic D, Grefen C, Schumacher K, Oecking C, et al. (2004) Visualization of protein interactions in living plant cells using bimolecular fluorescence complementation. Plant J **40**: 428–438

Wildermuth MC, Dewdney J, Wu G, Ausubel FM (2001) Isochorismate synthase is required to synthesize salicylic acid for plant defence. Nature **414**: 562–565

Wolinska KW, Vannier N, Thiergart T, Pickel B, Gremmen S, Piasecka A, Piślewska-Bednarek M, Nakano RT, Belkhadir Y, Bednarek P, **et al.** (2021)Tryptophan metabolism and bacterial commensals prevent fungal dysbiosis in Arabidopsis roots. Proc Natl Acad Sci **118**: e2111521118

Yang L, Chen X, Wang Z, Sun Q, Hong A, Zhang A, Zhong X, Hua J (2020) HOS15 and HDA9 negatively regulate immunity through histone deacetylation of intracellular immune receptor NLR genes in Arabidopsis. New Phytol **226**: 507–522

Yang L, Wang Z, Zhang A, Bhawal R, Li C, Zhang S, Cheng L, Hua J (2021) Reduction of the canonical function of a glycolytic enzyme enolase triggers immune responses that further affect metabolism and growth in Arabidopsis. Plant Cell http://dx.doi.org/10.1093/plcell/koab283

Zhang H, Zhang F, Yu Y, Feng L, Jia J, Liu B, Li B, Guo H, Zhai J (2020) A comprehensive online database for exploring~ 20,000 public Arabidopsis RNA-seq libraries. Mol Plant **13**: 1231–1233

Zhao Y, Hull AK, Gupta NR, Goss KA, Alonso J, Ecker JR, Normanly J, Chory J, Celenza JL (2002) Trp-dependent auxin biosynthesis in Arabidopsis: involvement of cytochrome P450s CYP79B2 and CYP79B3. Genes Dev **16**: 3100–3112

Zhou N, Tootle TL, Glazebrook J (1999) Arabidopsis *PAD3*, a gene required for camalexin biosynthesis, encodes a putative cytochrome P450 monooxygenase. Plant Cell **11**: 2419–2428

Zhou N, Tootle TL, Tsui F, Klessig DF, Glazebrook J (1998) *PAD4* functions upstream from salicylic acid to control defense responses in Arabidopsis. Plant Cell **10**: 1021–1030